Shore crabs reveal novel evolutionary attributes of the mushroom body

Nicholas James Strausfeld[1], Marcel Ethan Sayre[2]

[1]Department of Neuroscience, School of Mind, Brain and Behavior, University of Arizona, Tucson, United States; [2]Lund Vision Group, Department of Biology, Lund University, Lund, Sweden

Abstract

Neural organization of mushroom bodies is largely consistent across insects, whereas the ancestral ground pattern diverges broadly across crustacean lineages, resulting in successive loss of columns and the acquisition of domed centers retaining ancestral Hebbian-like networks and aminergic connections. We demonstrate here a major departure from this evolutionary trend in Brachyura, the most recent malacostracan lineage. Instead of occupying the rostral surface of the lateral protocerebrum, mushroom body calyces are buried deep within it, with their columns extending outwards to an expansive system of gyri on the brain's surface. The organization amongst mushroom body neurons reaches extreme elaboration throughout its constituent neuropils. The calyces, columns, and especially the gyri show DC0 immunoreactivity, an indicator of extensive circuits involved in learning and memory.

Introduction

Insect mushroom bodies, particularly those of *Drosophila*, are the most accessible models for elucidating molecular and computational algorithms underlying learning and memory within genetically and connectomically defined circuits (e.g., Aso et al., 2014; Senapati et al., 2019; Modi et al., 2020; Jacob and Waddell, 2020). An advantage of *Drosophila* is that it exemplifies a ground pattern organization that is largely consistent across hexapod lineages (Ito et al., 1998, 2014; Sinakevitch et al., 2001; Li and Strausfeld, 1997; Montgomery and Ott 2015; Groh and Rössler, 2011).

Because of the importance of mushroom bodies in understanding the relevance of synaptic organization in sentience and cognition, recognizing evolutionary divergence of these centers would be expected to yield experimentally testable predictions about evolved modifications of circuitry in relation to ecological demands imposed on the species. However, insect mushroom bodies show a remarkably conserved organization, which makes them

relatively unsuited for neuroevolutionary studies. There are some minor exceptions, to be sure: in honey bees and ants, calycal domains receive modality-specific afferents; in beetles, dietary generalists have more elaborate calyces than specialists; in aquatic beetles a modality switch has replaced olfactory input to a visual input into the calyces (Gronenberg, 2001; Farris and Schulmeister, 2011; Lin and Strausfeld, 2012). Less attention has been given to neural arrangements comprising the mushroom body lobes (columns), although some studies have addressed distinctions in basal groups such as silverfish (Zygentoma), dragonflies and mayflies (Farris, 2005; Strausfeld et al., 2009).

The evolutionary stability of the insect mushroom body contrasts with the recent demonstration that mushroom bodies of malacostracan crustaceans have undergone substantial and often dramatic modification of the mandibulate (ancestral) mushroom body ground pattern (Stegner and Richter, 2011; Wolff et al., 2015, 2017; Strausfeld et al., 2020). Whereas Stomatopoda (mantis shrimps), the sister group of Eumalacostraca, possesses mushroom bodies that correspond to those of insects, equipped with calyces from which arise prominent columns (Wolff et al., 2017), the trend over geological time has been a reduction of those columnar components such that the ancestral ground pattern organization of parallel fibers and orthogonal Hebbian networks has become morphed to provide planar arrangements within domed centers lacking columns (Wolff et al., 2015; Strausfeld and Sayre, 2019; Strausfeld et al., 2020). These neuronal adaptations nevertheless share the property with insect mushroom bodies of being immunopositive to an antibody raised against the catalytic subunit of protein kinase A, encoded by the *Drosophila* gene DC0, that is required for effective learning and memory (Kalderon and Rubin, 1988; Skoulakis et al., 1993). Antibodies raised against DC0 are reliable identifiers of neuropils mediating learning and memory both in arthropods and other phyla (Wolff and Strausfeld, 2012, 2015).

Whereas the evolutionary shift from columnar mushroom bodies to noncolumnar homologues is demonstrated across most decapod crustaceans, one lineage has until now defied unambiguous identification of a columnar or even a noncolumnar center. This is Brachyura, known in the vernacular as true crabs. Brachyura is a comparatively young lineage, recognized from fossils dating from the mid-Jurassic (Schweizer and Feldmann, 2010; Guinot, 2019). Phylogenomics places the origin of Brachyura also as mid-to-late Jurassic (Wolfe et al., 2019). Brachyura is the most species-rich decapod clade, comprising 6,793 currently known species (Ng et al., 2008). It is also a hugely successful lineage, extant species broadly distributed to occupy

58 benthic, littoral, estuarine, brackish, fresh water, terrestrial and even arboreal habitats. Many of
59 these ecologies are defined by complex topographies (Lee, 2015; Hartnell, 1988).
60 Historically, identifying a mushroom body homologue in the crab's brain has been
61 problematic. Claims for homologous centers range from paired neuropils in the brain's second
62 segment, the deutocerebrum, later attributed to the olfactory system (Bethe 1897), to an
63 insistence that the crab's reniform body is a mushroom body (Maza et al., 2016, 2020).
64 Demonstrated 132 years ago in stomatopod crustaceans, the reniform body is a morphologically
65 distinct center that coexists in the brain's lateral protocerebrum adjacent to its columnar
66 mushroom bodies (Bellonci, 1882; Thoen et al., 2019).
67 Until the present, observations of the varunid shore crab *Hemigrapsus nudus* have
68 identified large anti-DC0-reactive domains occupying almost the entire rostral volume of its
69 lateral protocerebrum but no evidence for mushroom bodies (Thoen et al., 2019). The affinity of
70 these domains to anti-DC0 suggested, therefore, a cognitive center far more expansive than
71 found in any other arthropod of comparable size, with the possible exception of the domed
72 mushroom body of the land hermit crab *Coenobita clypeatus* (Wolff et al., 2012). Here we
73 demonstrate that in the shore crab there are indeed paired mushroom bodies. But these have been
74 "hiding in plain sight," having undergone an entirely unexpected neurological transformation
75 that is opposite to the evolutionary trend shown in other lineages towards a domed noncolumnar
76 morphology.
77 Here we demonstrate evidence at level of neuronal arrangements showing that in the
78 shore crab paired mushroom bodies have undergone an evolved transformation that is possibly
79 unique to Arthropoda. They are inverted: their calyces reside deep within the lateral
80 protocerebrum, a location allowing outward expansion of the mushroom body columns which
81 reach expanded cortex-like folds beneath the brain's surface. The entire disposition of the shore
82 crab's mushroom bodies is opposite to that of any other crustacean, or insect, in which the
83 calyces are situated under the rostral surface of the lateral protocerebrum with their columns
84 extending downwards into deeper neuropil (Strausfeld et al., 2009; Wolff et al., 2017; Sayre and
85 Strausfeld, 2018).
86 Characters (traits) defining neuronal organization demonstrate that the mushroom bodies
87 of Stomatopoda phenotypically correspond to those defining the mushroom bodies of *Drosophila*
88 (Wolff et al., 2017). The following description of uses complementary methods that resolve
89 those traits in *Hemigrapsus nudus*. Reduced silver staining demonstrates spatial arrangements of

calycal and columnar neuropils and their detailed neuroarchitecture. Osmium-ethyl gallate treatment of intact brains resolves neuronal densities; and serial sections of these preparations provide the three-dimensional reconstructions shown throughout this account (see Methods). Golgi mass-impregnations enable crucial insights into the exceptionally elaborate organization of mushroom body intrinsic neurons, identified as the phenotypic homologues of insect Kenyon cells. Immunohistology has been used to resolve DC0-immunopositive components of the mushroom body calyces and columns, and antibodies raised against GAD (glutamic acid decarboxylase) reveal putative levels of local inhibition. Antibodies raised against tyrosine hydroxylase (TH) and 5-hydroxytryptophan (5HT) demonstrate arborizations consistent with those of output and input neurons intersecting different levels of the *Drosophila* and Stomatopod mushroom body columns.

We show that despite the varunid mushroom body's unparalleled intricacy and its unique transformation of the ancestral ground pattern, its defining traits nevertheless demonstrate phenotypic homology with the mushroom bodies of insects and those of other crustaceans. We close with a Discussion proposing that the evolution of such intricacy, and the expansion of the lateral protocerebrum to accommodate mushroom body enlargement, is likely to have contributed novel circuits and, ultimately, to cognitive flexibility permitting varunid Brachyura to exploit complex ecological topographies at interface of marine and terrestrial biotopes.

Results

The Results are organized into eight sections, the first describing the overall location and structure of the varunid mushroom body. This is followed by the identification of its neural components and their arrangements as elaborate networks comprising the paired calyces. Descriptions of the internal organization of the calyces' rostral extensions, and their two prominent columns, culminates with an explanation of the cortex-like organization of overlying gyri to which the columns project. The final observations address the relationship of the mushroom body to the reniform body, a center common to malacostracan crustaceans. To provide a three-dimensional understanding of this highly intricate system, descriptions refer to locations and arrangements within a reconstructed lateral protocerebrum and its major components (*see Methods*).

1. The varunid lateral protocerebrum (*Figures 1, 2, Figure 1 - figure supplement 1*)

In crabs, as is typical of stomatopods and most decapod crustaceans, the most anterior part of its brain, the protocerebrum, is flanked each side by a lateral outgrowth that expands into an enlargement of the eyestalk immediately proximal to the compound retina (*Figure 1 - figure supplement 1A*). This volume of brain comprises the lateral protocerebrum (*Figures 1A, 2A*). The lateral protocerebrum is connected to the midbrain proper by the eyestalk nerve composed of axons relaying information to and from the midbrain.

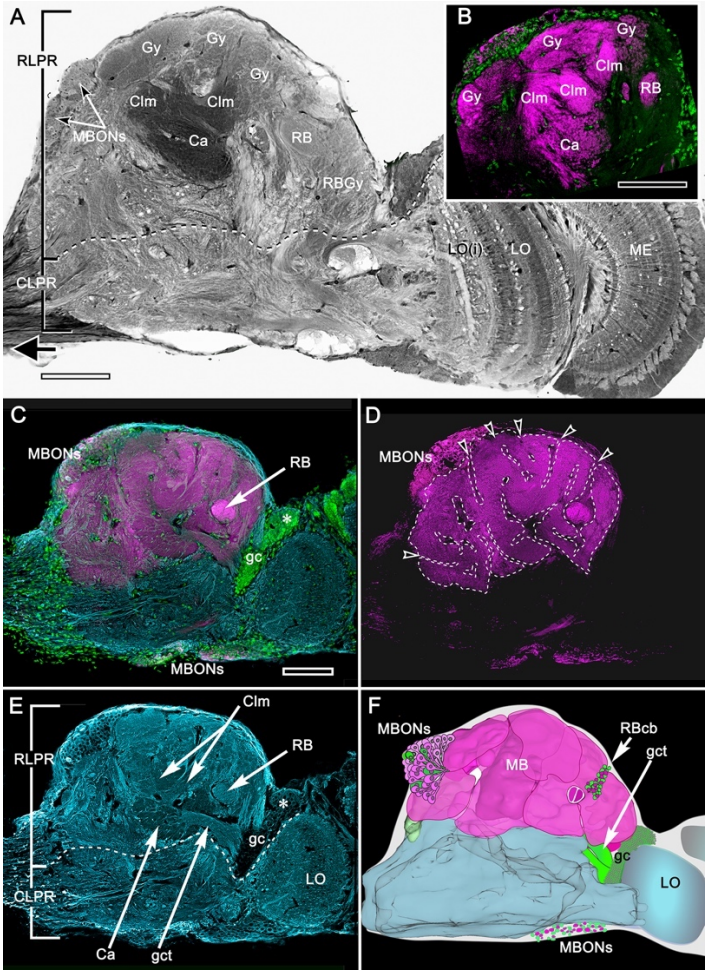

Figure 1. Organization of the varunid crab mushroom body and its associated gyri. (**A**) Brains treated with osmium-ethyl gallate demonstrate the overall disposition of neuropils, exemplified by this section of the lateral protocerebrum from its medial border to the optic lobe medulla. Its rostral domain (RLPR) includes the mushroom body calyces (Ca), columns (Clm) and their associated gyriform neuropils (Gy).Clusters of neuronal cell bodies (here MBONs) are distributed over the neuropil. Distal volumes of the RLPR are associated with the reniform body (RB; here its pedestal and a gyrus RBGy), which is situated between the mushroom body and the optic lobe, here represented by its medulla (ME) and bilayered lobula (LO, LOi). The optic lobe provides outputs to discrete neuropils comprising the caudal lateral protocerebrum (CLPR). (**B-E**) Anti-DC0-labelled (magenta) volumes in panel B match the corresponding membrane-dense calyces and columns and their rostral gyri in panel A. Panel C demonstrates that DC0-immunostained gyri occupy

almost the entire rostral level of the RLPR. Two small clusters caudally (MBONs) lining the CLPR, near the optic lobes, also include DC0-immunoreactive perikarya. The nuclear stain Syto13 (green) demonstrates the location of mushroom body globuli cells (gc) lying immediately beneath a group slightly large perikarya (asterisk). In panel D, removal of anti-□ tubulin and Syto13 labelling from C resolves the extent of the gyri and their many sulcus-like indentations (open arrowheads). In panel E anti-□□tubulin shown here alone resolves the overall fibroarchitecture of the LPR to provide correlative data with those provided by reduced silver stains (*Figure 2*). (**F**) Total Amira-generated reconstruction of a serial-sectioned, osmium-ethyl gallate treated eyestalk demonstrates the huge area of the lateral protocerebrum occupied by the folded gyri. Superimposed are the locations of small neurons supplying the reniform body (RBcb), mushroom body globuli cells (gc) and their tract of neurites leading to the calyx (gct), here obscured by overlying gyri. Scale bars, A, B, 100μm; C-F, 100μm.

Figure 1 —— figure supplement 1. Schematic of the *Hemigrapsus* brain

Brains treated with osmium-ethyl gallate or with reduced silver (*Figures 1A, 2A*) resolve the varunid lateral protocerebrum as a hump-shaped volume divided into a rostral and caudal part. The rostral lateral protocerebrum (RLPR), once referred to as the terminal medulla, a now defunct term (Strausfeld, 2020), is dominated by two centers: the mushroom bodies and the smaller reniform body. There is a small number of other satellite neuropils near the origin of the eyestalk nerve. The mushroom body is immediately recognizable by its intensely osmiophilic calyces from which arise columns that extend outwards, branching into a cortex-like neuropil composed of gyri (*Figure 1A*). These occupy the outermost volume of the RLPR. The reniform body comprises an independent system of interconnected neuropils situated laterally constrained to a volume of the RLPR that extends from its dorsal to its ventral surface (Thoen et al., 2019). In longitudinal sections of the RLPR, its prominent axon bundle, the pedestal, is seen in cross section(*Figures 1A, 2A*). The crab's RLPR corresponds to that volume of the insect protocerebrum containing the mushroom body and its immediate associated neuropils, such as the lateral horn (*Figure 1 - figure supplement 1B, C*).

As in stomatopods and decapods, the crab's RLPR receives terminals of olfactory projection neurons originating from both the ipsi- and contralateral olfactory (antennular) lobes located in the brain's second segment, the deutocerebrum (*Figure 1 - figure supplement 1A*). The axons of more than a thousand projection neurons are organized into several discrete fascicles bundled together to provide the antennoglomerular tract (AGT). The left and right AGTs extend superficially across the midbrain to meet just dorsal to the central body. There, each tract bifurcates to provide inputs to each lateral protocerebrum from both the ipsi- and contralateral olfactory lobes (*Figure 1 - figure supplement 1A*). The eyestalk nerve also carries other efferent axons to the lateral protocerebrum: these include relay neurons from other sensory neuropils,

175 relays from the opposite lateral protocerebrum and optic lobes, and interneurons relaying from
176 various midbrain neuropils.
177 The caudal volume of the lateral protocerebrum (CLPR) is mainly associated with
178 outputs from the optic lobe neuropils (*Figure 1A*). Most of these originate from the lobula, each
179 bundle of outgoing axons representing a population of one of the numerous morphological types
180 of columnar neurons. Bundles segregate to a system of interconnected neuropils called optic
181 glomeruli, as occurs in insects (Okamura and Strausfeld, 2007). Further relays from the
182 glomeruli send information centrally to the midbrain via the eyestalk nerve. The nerve also
183 carries to the midbrain the axons of neurons from the lateral protocerebrum's rostral neuropil, the
184 mushroom bodies, and its associated gyri and from CLPR neuropils associated with the optic
185 glomeruli.
186
187 **2. Organization of DC0-positive volumes (*Figure 1*).**
188 The dense osmiophilic calyces and their extended columns (*Figure 1A*) correspond to discrete
189 neuropils showing high levels of immunoreactivity to antibodies raised against DC0 (*Figure 1B*).
190 The fibroarchitecture of these DC0-positive volumes is revealed by labeling with antibodies
191 against α-tubulin or by reduced silver. (*Figures 1E; 2A-C*) that provide correlative data for
192 resolving and interpreting the arrangements of the mushroom body volumes in 3-D
193 reconstructions (*Figure 2 - figure supplement 2*: see Methods). Salient both in osmium–ethyl
194 gallate-stained brains is the layer of gyri that defines the outer level of the rostral lateral
195 protocerebrum (*Figures 1A, 2D, E*). Gyri are DC0-immunoreactive and are contiguous with each
196 of the DC0-immunoreactive columns that extend outwards from the calyces. Gyri are resolved as
197 pillowed folds and indentations (sulci: *Figure 1D, F*) comparable to the folded architecture of a
198 mammalian cerebral cortex. This feature appears to be unique to Brachyura (see Discussion).
199
200 **3. The calyces and their origin from globuli cells (*Figures 1, 2*)**
201 If centers are claimed as phenotypic homologues of insect mushroom bodies, then the centers are
202 expected to have the following categories of neurons irrespective of their divergence from the
203 ancestral ground pattern as represented in the allotriocarid clade Cephalocarida (Stegner and
204 Richter, 2011). These categories are: 1) intrinsic neurons, the most populous of which are
205 Kenyon cells defining the mushroom body's volume, shape, and subdivisions; 2) extrinsic
206 neurons providing inputs from sensory centers (Kanzaki et al., 1989; Lin and Strausfeld, 2012;

Li et al., 2020), as well as protocerebral regions encoding high level multisensory information (Li and Strausfeld, 1999); and 3) output neurons that encode information computed by levels of the mushroom body lobes (Li and Strausfeld, 1999; Turner et al., 2008). The latter are referred to here as MBONs, adopting the term from studies on *Drosophila* (Aso et al., 2014a,b).

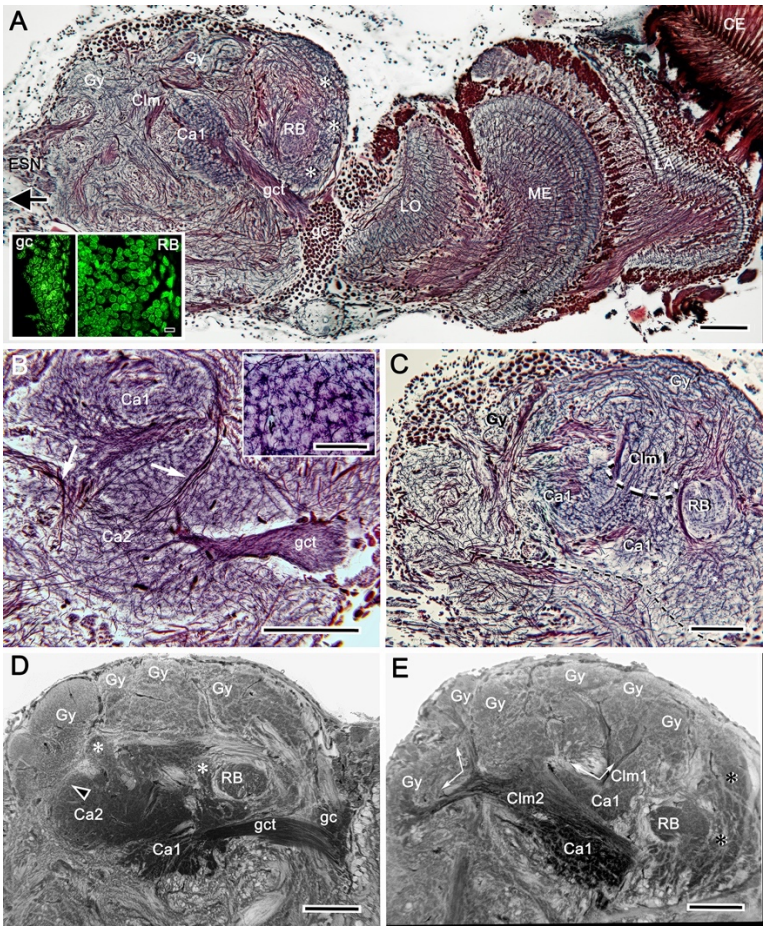

Figure 2. Uniquely identifiable neuropils of the mushroom bodies are resolved by reduced silver. (**A**) Horizontal section of the lateral protocerebrum demonstrating the more dorsal of the two calyces (Ca1) and its supply by the globuli cell tract (gct) from the cluster of globuli cells (gc). Columnar extensions (Clm) from the calyces reach out to overlying gyri (Gy). The reniform body is shown with three of its gyri (asterisks) and its bundled axons (RB) situated between the mushroom body and optic lobes, insets lower left compare the smallest perikarya supplying the calyces (globuli cells, gc) with the next smallest perikarya belonging to neurons of the reniform body (see *Figure 2 -figure supplement 1*). Abbreviations: ESN, eyestalk nerve; CE, compound retina, LA, lamina, ME, medulla; LO, lobula. (**B**) Adjacent calyces (Ca1, Ca2) showing their diagnostic arrangement of microglomeruli (inset upper right; see also Figure 3). Arrows indicate afferent fibers into Ca2 from nonolfactory origins. (**C**) The calycal origin and rostral extension of the Ca1 column (encircled). At this level, penetration by en passant axon bundles causes the calyx to appear fragmented. (**D, E**) Osmium ethyl gallate-treated sections at two depths. Panel D indicates the bulk and elaboration of calycal neuropils. At this level calyx 2 appears as the larger. The arrowhead indicates the root of column 2. Calyx 1 is shown with its globuli cell tract entering a domain denoted by lateral extensions of calyx 1. In panel E, the base of column 1 (Clm1) is shown arising from Ca1, its curvature at this level splitting it into two parts. Column (Clm2) is shown extending two branches into the gyriform layer above. Clm1 extends outwards just proximal to the pedestal of the reniform body

229 (RB). In addition to columns, calyces provide occasional narrower finger-like extensions extending
230 towards the gyri (asterisks in D). Scale bars, 100μm. Inset in A, 10μm, inset in B, 50μm.
231 **Figure 2 —— figure supplement 1.** Globuli cells supplying intrinsic neuron to the mushroom bodies
232 **Figure 2 —— figure supplement 2.** Globuli cells provide two tracts, one to each calyx.
233

234 Intrinsic neurons supplying the *Hemigrapsus nudus* calyces correspond to insect Kenyon
235 cells. As do insect Kenyon cells, these originate from the brain's smallest and most crowded
236 population of neuronal cell bodies, the globuli cells (*Figures 1C, 2A,D, Figure 2 – figure*
237 *supplement 1*). In other arthropods globuli cell perikarya have been shown as dense clusters
238 situated at the rostral surface of the lateral protocerebrum, usually near its proximal margin or
239 immediately above the mushroom body calyces, as in *Drosophila* or Stomatopoda, or, in
240 malacostracans with eyestalks, close to the lateral protocerebrum's attachment to the eyestalk
241 nerve. In *H. nudus*, however, globuli cell perikarya are found in a completely different and
242 surprising locality: a densely populated "hidden" volume tucked between the proximal margin of
243 the lobula and the most distal border of the lateral protocerebrum (*Figure 2A*). As in other
244 pancrustaceans these perikarya are the smallest perikarya of the brain, in the varunid ranging
245 from 5 to 7 μm in diameter (compared in *Figure 2A, inset, Figure 2 – figure supplement 1*). In
246 crabs used for these studies (carapace widths of 4-8 cm), we estimate that this perikaryal cluster
247 accounts for 22,000 mushroom body intrinsic neurons shared by the two calyces (see Methods).
248 Cytological distinctions amongst cells in the cluster, denoted by their appearance after osmium-
249 ethyl gallate staining (Wigglesworth, 1957), suggest that new globuli cells are being
250 continuously generated from ganglion mother cells situated at the cluster's periphery (*Figure 2 -*
251 *figure supplement 1D-G*).

252 Cell body fibers (neurites) extending from the globuli cell cluster are tightly packed into
253 two prominent bundles, called globuli cell tracts, one projecting obliquely ventrally the other
254 obliquely dorsally to supply each of the two adjacent calyces (*Figure 2A, B, D - figure*
255 *supplement 2*). Neurites comprising these tracts fan out to supply each calyx with its ensembles
256 of mostly orthogonally arranged dendritic networks that interweave amongst a mosaic of
257 microglomeruli (*Figure 2B; Figure 3A, B, - figure supplement 1*). The networks, which are
258 resolved by silver stains, comprise overlapping populations of intrinsic neuron processes
259 extending amongst a mosaic of many thousands of discrete microglomeruli (*Figures 2B, 3A*).
260 These are assumed to be sites of synaptic convergence (*Figure 3- figure supplement 1*),
261 corresponding to microglomerular organization in the calyces of insect, stomatopod and caridean

262 mushroom bodies (Yasuyama et al., 2002; Sjöholm et al., 2006; Groh and Rössler, 2011; Wolff
263 et al., 2017; Sayre and Strausfeld, 2019). As will be described in the following section,
264 components of microglomeruli include the terminals of afferent relays originating from the
265 olfactory lobes, neuropils associated with the visual system, including the reniform body, and
266 centrifugal neurons from the midbrain.
267 Serial sections oriented horizontally, approximately parallel to the rostral surface of the
268 protocerebrum and stained with reduced silver, suggest the calyces are planar neuropils (*Figure*
269 *2B*). But this is deceptive, as shown by sections in the vertical plane demonstrating how the deep
270 calycal cytoarchitecture extends rostrally to merge with the base of its column(*Figure 2C*). The
271 total extent and volume of calycal neuropil is surprisingly large as can be seen in intact brains
272 treated with osmium-ethyl gallate, a technique that selectively colors cell membranes black
273 (Wigglesworth, 1957). The method reveals volumes of neuropil in shades of black to light gray,
274 the darker the neuropil, the more densely packed its neuronal processes (*Figures 1A, 2D, E;*
275 *Figure 4A, figure supplement 1*). This density is a reflection of the many thousands of intrinsic
276 neurons comprising the calyces. Volumes that are paler are composed of neuronal processes that
277 are stouter and contribute less stainable membrane, as in the overlying gyri.
278 Computer-generated reconstructions and rotations of osmium-ethyl gallate stained
279 sections (see Methods) demonstrate that the calycal volumes are topographically elaborate
280 (*Figure 2 supplement 2*); each calyx is stratified at deeper levels of the lateral protocerebrum's
281 rostral volume, but where calycal neuropils extend rostrally their upper borders are defined by
282 irregular arrangements of small peaks and troughs. Two prominent columns, one from each
283 calyx, extend outwards into the overlying gyri (*Figure 2E*). Reduced silver material and Golgi
284 impregnations resolve their elaborate internal organization (*Figure 2C*), which is described in
285 section 5, below.
286
287 **4. Neuronal organization of the calyces (Figures 3-6)**
288 Intrinsic neuron processes and terminals of efferent neurons are the main constituents of the
289 varunid calyces (*Figure 3B, Figure 3 - figure supplement 1; Figure 4B-G, Figure 4 - figure*
290 *supplement 1*). They receive inputs from neurons primarily from the deutocerebrum (*Figure 3 –*
291 *figure supplement 1B*) but also from the optic lobes and from its associated neuropils, such as the
292 reniform body (*Figure 4 - figure supplement 2*), as also shown for Stomatopoda (Thoen et al.,
293 2019). Golgi impregnations and osmium-ethyl gallate demonstrate that calyces, across their

horizontal and vertical extent, are composed of discrete domains of morphologically distinct networks comparable to the discrete modality-specific zones of Kenyon cell dendrites that define the insect calyces (Ehmer and Gronenberg, 2002; Strausfeld, 2002).

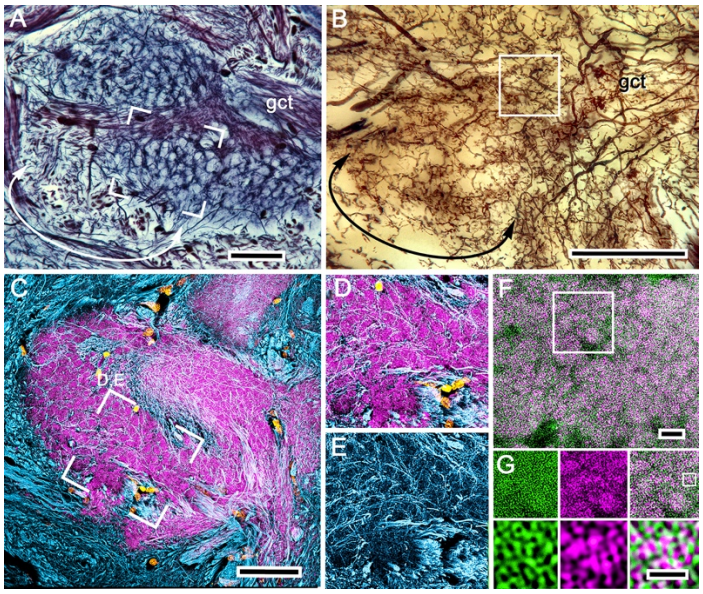

Figure 3. Organization of calyx 1: microglomeruli. (**A**) Reduced-silver-stained calyx showing its globuli cell tract (gct) with, at a different level, many of its constituent neurites giving rise to branches that delineate the mosaic organization of microglomeruli. (**B**) Golgi impregnations provide examples of intrinsic neurons, the branches and fine processes of which extend through domains of the calyx that correspond to those revealed both by reduced silver and by antibodies against DC0. A subfield (curved double arrow) in panel A corresponds to the denoted branches of the illustrated intrinsic neuron in panel B. (**C**) Microglomeruli are specifically labelled by anti-DC0. Microglomerular size and density in the boxed area corresponds to an equivalent microglomerular organization identified by reduced silver (boxed areas in A). (**D-G**) The mosaic is also reflected by the pattern of all intrinsic neuron processes at that level revealed by anti-α–tubulin; these enwrap DC0-positive microglomeruli (D, E). The same system of microglomeruli is resolved using combined actin/anti-synapsin. The area identified in a field of Golgi-impregnated intrinsic neuron processes (boxed in B) is equivalent to the area of the calyx in panel F labelled with actin/anti-synapsin demonstrating the microglomerular mosaic. The boxed area in F is shown in panel G. (**G**) The upper row shows actin and synapsin separate, with the superimposed images in the right panel in G). The boxed area in the upper right panel of G indicates a single microglomerulus. This is enlarged in the lower three panels of G, again showing actin and synapsin as separate images and then combined lower right to demonstrate the density of synapsin-labelled profiles, and thus direct evidence of massive convergence at a calycal microglomerulus (panel G). Scale bars, A–C, 50μm; F, 10μm; G, 2μm.

Figure 3 —— figure supplement 1. Rectilinear network organization of the calyx and afferent supply.

Most calycal neuropil is characterized by its dense arrangement of small almond-shaped subunits (*Figure 3A*), here referred to as microglomeruli following the term given to comparable elements described from insect mushroom body calyces (Yasuyama et al., 2002 Sjöholm et al., 2006; Groh and Rössler, 2011). However, some peripheral volumes of the calyces comprise more distributed arrangements (*Figure 3A,B*). These appear to receive terminals from axons of

relay neurons emerging from fascicles in the eyestalk nerve that are not part of projections from the olfactory lobes (*Figure 2,B)*.

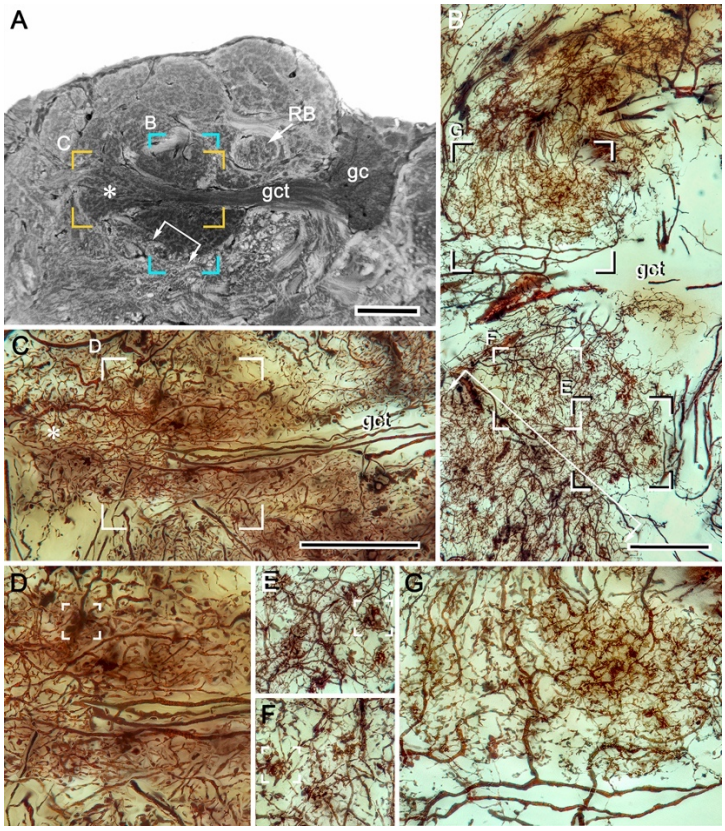

Figure 4. Intrinsic cell dendrites define calycal territories. (**A**) Osmium-ethyl gallate resolves calycal territories matching the dendritic fields of morphologically distinct intrinsic neurons. Letters in panel A indicate panels showing corresponding locations of Golgi-impregnate dendritic fields shown in B and C. Boxed areas in B and C are enlarged in panels D–G to demonstrate distinctive dendritic morphologies. The locations of the arrowed bracket and asterisk in A correspond to their locations in B (the bracket) and C (the asterisk). These further indicate the fidelity of calyx organization indicated by these two histological methods. Open boxes in panels D–-F indicate different morphological specializations of afferent terminals. Abbreviations: RB, reniform pedestal; gc, globuli cells; gct, globuli cell tract. Scale bars, A, C, 100μm, B, 50μm.

Figure 4 —— figure supplement 1. Fidelity of intrinsic neurons fields

Figure 4 —— figure supplement 2. Calyx distinctions

Discrete fields comprising intrinsic cell processes are recognized by their distinctive and particular morphologies (*Figure 4B–G, Figure 4 – figure supplement 1*). Each morphological type is defined by the patterning of its initial branches from its globuli cell neurite and the subsequent reticular trajectories made by their tributaries down to the details of their final specializations. The latter indicate points of functional connection and are morphologically comparable to the claws, clasps and dendritic spines that decorate the dendritic branches of

Kenyon cells in *Drosophila* and other insects (Ito et al., 1998; Strausfeld and Li, 1999; Strausfeld 2002) and the dendrites of homologous intrinsic neurons in the mushroom bodies of marine hermit crabs (Strausfeld and Sayre, 2019). As in those taxa, in the varunid calyx these specializations invariably relate to the distribution and patterning of its microglomeruli (*Figure 3A,B*).

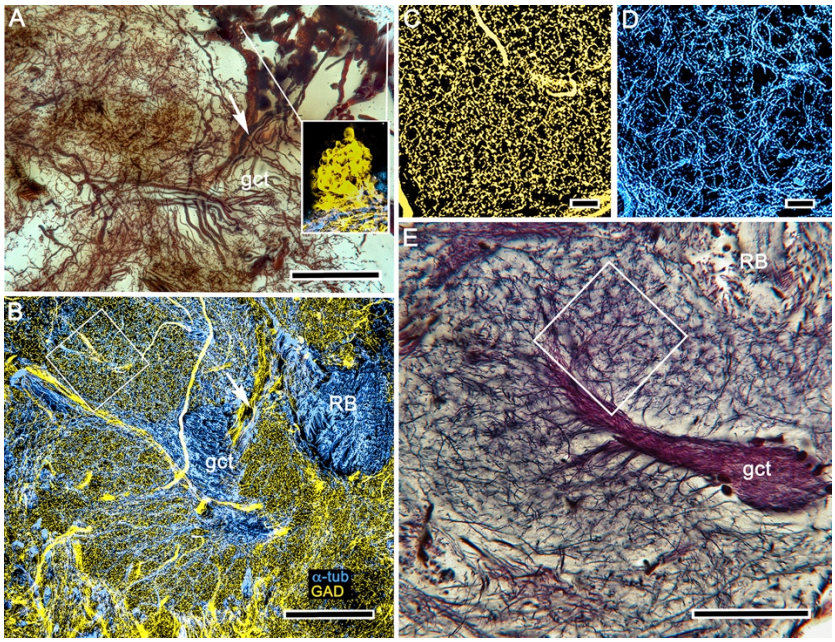

Figure 5. Evidence for local inhibition in the calyx by anaxonal neurons. (**A**) 40-50 large perikarya situated rostrally above the gyri are immunoreactive to glutamic acid decarboxylase (GAD, as shown in the right inset. These neuron cell bodies, which are here Golgi–impregnated, send stout cell body fibers (arrow) to the calyces where they provide widely branching and extremely dense processes that do not follow the patterns of the microglomerular mosaic. (**B**) GAD immunoreactivity reveals their branches and finest processes spreading through every calycal domain and hence positioned to potentially interact with all the intrinsic neuron dendritic fields. (**C, D**) GAD immunoreactivity in an area shown by the box in panel B, and an equivalent area in panel E showing the mosaic of microglomeruli. This mosaic is also evident from the pattern a α-tubulin-immunoreactive intrinsic neurons shown in D (same boxed area in B Scale bars, A, B, 100μm, C, D, 10μm, E, 50μm.

Microglomeruli revealed by reduced silver beautifully match the size and mosaic arrangement of microglomeruli resolved by their intense immunoreactivity to antibodies raised against DC0 (*Figure 3 A–C*). The bundled branches of intrinsic neurons resolved by antibodies against α-tubulin (*Figure 3D,E*) further resolve microglomeruli as participants of an elaborate organization of orthogonal networks that correspond to distinct morphological types of intrinsic neurons revealed as single cells by Golgi-impregnation (*Figure 4B,C, Figure 4 - figure supplement 1*). Each glomerulus signifies the site of an incoming terminal's presynaptic bouton

368 or varicosity (*Figure 3 - figure supplement 1*). Combined anti-synapsin immunoreactivity and F-
369 actin labelling (*Figure 3F-G*) further demonstrates the profusion of postsynaptic sites belonging
370 to intrinsic neurons that converge at each microglomerulus. The densely packed presynaptic
371 specializations further confirm the status of a microglomerulus as the site of massive transfer of
372 information from presynaptic terminals onto many postsynaptic channels.

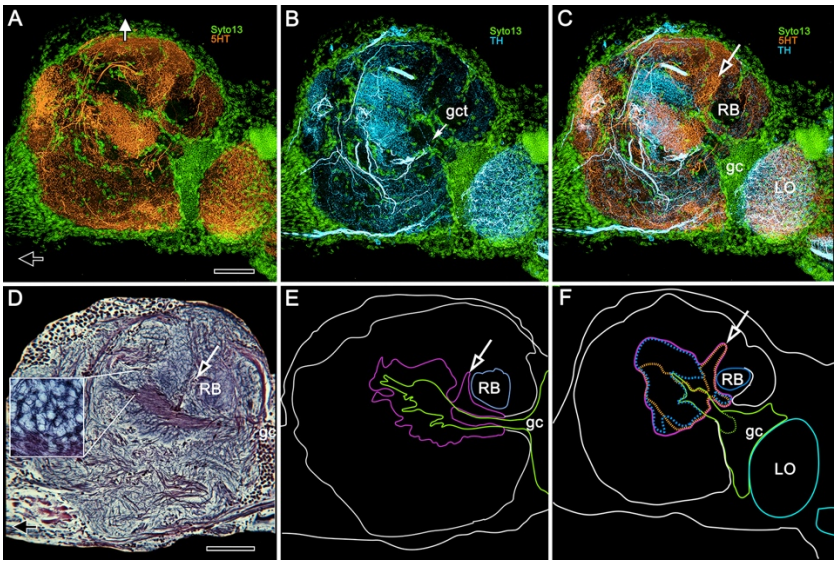

373

374 **Figure 6. 5HT and TH immunoreactivity define different calycal domains.** (**A,B**) Although many
375 volumes of the lateral protocerebrum are distinguished by 5HT (panel **A**, 5 hydroxytryptophan, orange)
376 immunoreactivity, the densest system of branches is in a rostral domain of calyx 1. TH (panel **B**, tyrosine
377 hydroxylase, cyan) defines two domains, one partially overlapping 5HT, the other not (panel **C**). (**D**) Bodian
378 silver-stained calyx 1 showing its distinctive microglomerular mosaic (inset). (**E**) Outlined in purple is the
379 total calycal perimeter at this level of sectioning and orientation. The open arrow indicates the origin of
380 column 1. (**F**) Perimeter (purple) of calyx 1 in a section of the RLPR slightly rotated around its lateral-medial
381 axis, mapping within it 5HT- and TH- immunoreactivity (as in panels A–C) also indicating the origin of
382 column 1 (open arrow, as in panel C). Abbreviations: RB, reniform body; gc, globuli cell cluster; gct, globuli
383 cell tract; LO, lobula. Scale bars for all panels, 100μm.
384

385 As remarked, the shapes and arrangements of intrinsic neurons and their synaptic
386 specializations contribute to orthogonal networks in the calyces and define calycal domains.
387 However, the domains are not arranged as neatly adjacent territories as in the insect calyx
388 (Gronenberg, 2001). Instead, the varunid calyx can reveal domains that extend vertically or
389 horizontally (*Figure 3 - figure supplement 1*), or comprise unexpectedly elaborate arrangements
390 that are understood only after they are matched to an appropriately oriented osmium-ethyl gallate
391 section (*Figure 4A,B, figure supplement 1*). One of the most challenging of these arrangements
392 consists of a population of intrinsic neurons defining a cylindrical domain that splays out as it
393 extends towards the proximal margin of the lateral protocerebrum (*Figure 4A*). The entire

394 ensemble comprises densely branched narrow-field arborizations that surround the initial
395 branches of a subset of globuli cell neurites (*Figure 4A,C,D*). The core leads to a terminal
396 expansion that is confluent with the base of one of the two large columns that extends to the
397 overlying gyri. Serial reduced-silver sections reveal this as originating only from calyx 2,
398 indicating that calyx 2 differs from calyx 1 with regard to at least one population of intrinsic
399 neurons. As in many insect lineages where there are paired calyces, it is such subtle distinctions
400 that demonstrate disparate organization across paired calyces (Farris and Strausfeld, 2003).
401 Reduced-silver stains showing axon tracts reveal inputs to calyx 2 originating from a tract that
402 recruits its axons from the reniform body and the medulla. Collaterals from this tract spread into
403 a deep level of calyx2 neuropil where they spread across microglomeruli bordering one side of
404 the incoming neurites from the globuli cell tract (*Figure 4 - figure supplement 2*). The
405 correspondence of this arrangement with insect calyces is considered in the Discussion.
406 There is one critical exception to the generalization that calycal subdivisions are denoted
407 by different types of intrinsic neurons. The exception is that there is a system of neurons that
408 arborizes uniformly throughout both calyces. These arborizations belong to GAD-
409 immunoreactive local processes originating from a dorsal cluster of large cell bodies, each of
410 which provides an anaxonal field that arborizes throughout both calyces, and into each of its
411 domains. (*Figure 5A,B*). These densely packed processes are exceptional in that they do not obey
412 the orthogonal leitmotif of the calyx, as revealed by anti-a-tubulin (*Figure 5C, D*), nor do they
413 reflect the mosaic arrangement of glomeruli (Figure *5C-E*). Instead, anti-GAD-immunoreactive
414 branchlets populate all the calycal domains and do so in great numbers, the totality suggesting
415 that local inhibitory elements are distributed amongst all intrinsic cell processes irrespective of
416 whether they are in immediate proximity to or distant from a microglomerulus (*Figure 5 C-E*).
417 Whereas GAD immunohistology does not distinguish local calycal domains, these are
418 indicated by the inhomogeneity of fields of 5HT- and TH-immunoreactive across the calyces
419 (*Figure 6*). The neurons providing these fields also appear to be specific to the calyces and not
420 part of a wider system that extends to other regions of the LPR. Those more distributed systems
421 include densely branched arborizations that populate the optic lobe's lobula and 5HT-
422 immunoreactive neurons that arborize in certain neuropils of the CLPR as well as gyri. These are
423 likewise distinct from the 5HT and TH-immunoreactive fields that intersect the mushroom body
424 columns, which are described next.

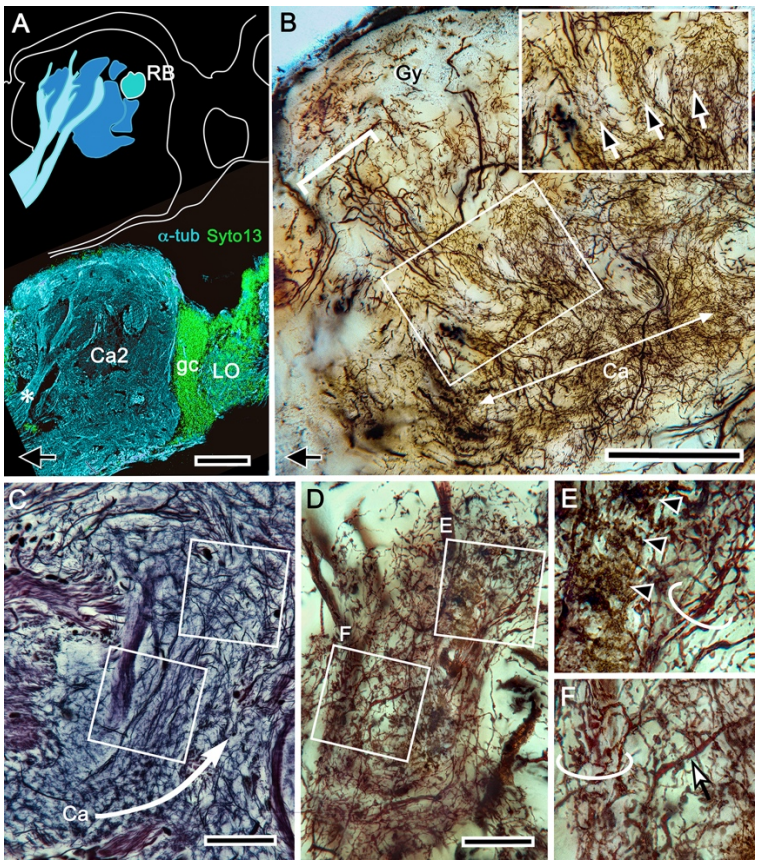

Figure 7. Origin of calycal extensions and columns. (**A, B**) Anti-α–tubulin (cyan) reveals the organization of large fiber bundles and coarse neuropil but, at low magnification, shows neuropils of the calyces as almost featureless (panel A). Part of the calyces are penetrated by incoming tributaries from the eyestalk nerve (asterisk in A, lower panel). A corresponding Golgi-impregnated region (B) demonstrates a system of medium-diameter branched processes that provide fine networks enwrapping the origin of columns. Some networks also extend as finger-like extensions outwards from the calyces. Panel B shows one column (upper left bracket) the base of which is flanked by those arrangements (enlarged in upper right inset indicated by arrows). This extensive system of processes does not derive from the globuli cell clusters although it is clearly associated with the entire extent of the calyces, suggesting a possible role in calyx-wide modulation. (**C-D**) As shown by this reduced silver stained section, the column arising from calyx 1 is extremely elaborate, comprising at least two longitudinal divisions each defined by arrangements of intrinsic neuron processes and their branched specializations. The curved arrow in panel C indicates the continuation of intrinsic neuron microglomeruli for a short distance alongside the column. The boxed areas in panel C, indicate corresponding levels identified in a Golgi-impregnated column 1 (D) showing enlargements in panels E, F, of their constituent arrangements. In panel E ascending fibers provide short collaterals (arrowheads) across one longitudinal subdivision of the column. In another subdivision, ascending intrinsic processes are arranged as a tangle (circled in panels E, F). Panel F also shows a large beaded branch (arrowed) of a mushroom body input neuron (MBIN) extending into the column. Abbreviations: RB, reniform body; Ca2, calyx 2; gc, globuli cells; LO, lobula; Gy, gyri. Scale bars, A, B, 100μm; C, D, 50μm.

Figure 7 —— figure supplement 1. Intrinsic neuron organization in columns

Figure 7 —— figure supplement 2. The interface between columns and gyri.

450 **5. Transition from the calyces to the columns**

451 Thus far we have demonstrated the composition of the calyces by approximately orthogonal
452 networks provided by intrinsic neurons and their arrangements with microglomeruli.

453 Stomatopod and shrimp mushroom bodies demonstrate a clear transition of neuronal
454 organization between the calyx and its columnar extensions (Wolff et al., 2017; Sayre and
455 Strausfeld, 2018). In *H. nudus* there is no abrupt transition (*Figure 2)*. This ambiguity is
456 seconded in brains treated with osmium-ethyl gallate, which show lateral protocerebral neuropil
457 supplied by globuli cell neurites gradually fading from black to gray, signifying decreasing
458 densities of neuronal membrane, finally giving way to the uniformly pale aspect of the overlying
459 gyri (*Figure 1A, Figure2D,E*). 3-D reconstructions of the dark volumes show a layered
460 arrangement at deeper layers of the calyces changing to a more corrugated appearance,
461 particularly at its outer surface (*Figure 2, supplement 2*). Silver impregnations show that the base
462 and some of the initial length of a column are clearly reticulated (*Figure 7C*). Double Golgi
463 impregnation shows that these networks receive contributions from two sources: the extensions
464 of axon-like processes from intrinsic neuron fields in the calyx; and intrinsic arborizations, many
465 extremely complicated, that originate from thin neurites, presumed to belong to globuli cells
466 (*Figure 7 - figure supplement 1*). An additional system of networks extends outwards to flank
467 each calyx's column (*Figure 7B*). These reticulations originate from a tangle of processes
468 situated at a deeper level of the calyces (*Figure 7B*) that does not reflect any relationships with
469 microglomeruli. The likely origin of this system (*Figure 7B*) is not from globuli cells but from a
470 small clusters of cell bodies, some DC0-immunoreactive, situated ventrally close the inner
471 margin of the lobula (*Figure 1C*). We interpret this tangle of processes (*Figure 7B*) as belonging
472 to interstitial local interneurons providing elements to the columns at a level limited to their
473 emergence from the calyces a small part of their initial length. The topology of these
474 arrangements, including the small column-specific intrinsic arborizations (*Figure 7 - figure*
475 *supplement 1E-K*) is reminiscent of interstitial neurons interposed between the calyces and
476 pedunculus of the honeybee (Strausfeld, 2002).

477 The origin of the columns and smaller extensions from the calyces are further
478 demonstrated by selected levels of silver-stained brains. Serial sections resolve the uneven rostral
479 border of the calyces and the two columns reaching outwards towards the overlying gyri (*Figure*
480 *7 - figure supplement 2*). The series also demonstrates the fidelity of silver and osmium-ethyl
481 gallate in showing corresponding origins of the columns from the two calyces. These aspects

482 emphasize that the seemingly irregular morphology of the rostral part of the calyces is not
483 irregular by happenstance but is a defining feature of the lateral protocerebrum.
484 Reduced silver preparations demonstrate that a column is subdivided into parallel
485 components as in insect mushroom bodies, where each subdivision has a distinctive arrangement
486 of intrinsic neurons (Strausfeld et al. 2005; Sjöholm et al., 2005; Tanaka et al., 2008) and is
487 defined by distinctive patterns of gene expression (Yang et al., 1995). What is unexpected is the
488 degree of elaboration observed in the varunid mushroom body. Golgi impregnations demonstrate
489 that, compared with other pancrustaceans, mushroom bodies in a crab are stunningly complex,
490 both with regard to their calyces and columns. The varunid's columns consist of parallel intrinsic
491 cell fibers that are almost obscured by numerous other arrangements, the variety of which is
492 compatible with the variety of their morphological fields in the calyces. Comparison of the
493 silver-stained column originating from calyx 2 to one impregnated by mass Golgi impregnations
494 (*Figure 7C,D*) demonstrates a discrete and complicated system of processes, some providing
495 bridgelike connections across them (*Figure 7E*), others having irregular branches, lateral
496 prolongations, and bundled parallel fibers (*Figure 7E,F*). In addition, larger dendrite-like
497 elements arising from stout processes within the columns suggest that those processes may
498 provide outputs extending outwards to the overlying gyri (*Figure 7D,F*), a feature to which we
499 return in section 7.
500 Golgi impregnation has its own peculiar limitations: it is stochastic, revealing probably
501 less than 1% of the total population of neurons, even after double impregnation. Nevertheless,
502 mass impregnation further suggests that the columns from the two calyces are not identical.
503 Although networks of intrinsic cells in both columns receive terminals from branches of the
504 olfactory glomerular tract, there are clear differences between the columns from calyx 1 and
505 calyx 2. Column 2 is broader and more difficult to discern in reduced silver. In part because
506 many of its intrinsic processes are all extremely thin, many less than a micron in diameter (see
507 section 7 below). At first sight, the organization of processes comprising column 2 appears to be
508 chaotic. However, when scrutinized more closely the organizations of its dendrites and
509 collaterals contribute to subsets of different arrangements disposed across the width of a column
510 and at different levels along it (*Figure 7 supplement 1A-C*). Reciprocal channels to the column
511 from the gyri are suggested by the presence of descending axons flanking the column, providing
512 varicose collaterals into it (*Figure 7 - figure supplement 1A*). These varieties of columnar
513 arrangements are further considered in the Discussion.

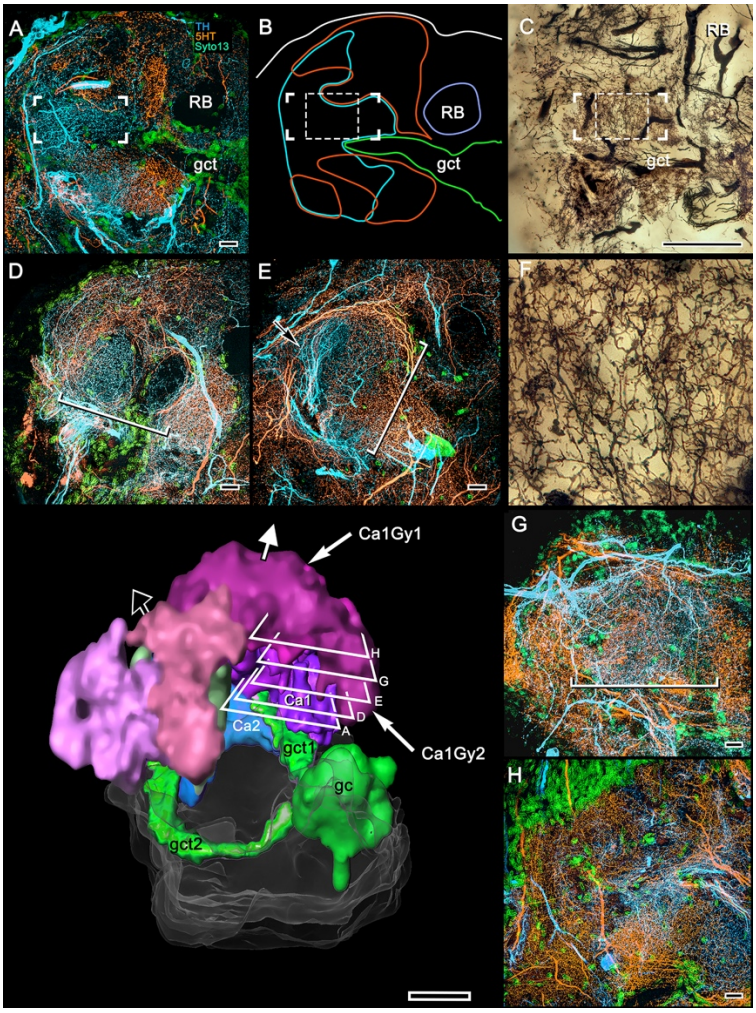

Figure 8. **5HT and TH immunoreactivity resolve different levels in the calyx 1 column.** Looking downwards through the rostral surface of LPR**,** this sequence of confocal slices (**A,D,E,G,H**) shows views starting at the column's origin from calyx 1 (panel **A**) then following its outward passage rostrally to the level at which the column merges with the overlying gyri (panels **G**, **H**). (**B)** shows outlines of 5HT- and TH-immunoreactive fields at level A in relation to the globuli cell tract (gct, green) and the cross section of the reniform body's pedestal (RB).The dendritic field of a TH-immunoreactive cell is bracketed in A,B and a smaller portion of it is denoted by a dashed square in B. (**C**) Golgi preparation of dendrites in area equivalent to bracketed and dashed areas in (B) show that at this level, networks of intrinsic neurons have given way to more loosely defined reticulations. (**F**) Enlargement of dashed square in (C). At the level shown in panel A, 5HT- and TH-immunoreactive fields are segregated across the origin of the column and continue to be, at least until the level shown in panel **E**, suggesting 5HT- and TH-immunoreactive fields are restricted to the column's longitudinal subdivisions. TH-immunoreactive fields can be noticeably clustered within a small area of the column's cross-section (arrow in E) as are MBONs in *Drosophila* mushroom bodies. The width of the column (brackets in panels D, E, G) increases gradually through layers **D**, **E**, and **G** (see brackets), and in the gyrus (**H**) its borders are no longer distinguishable. The 3–D reconstruction (lower left) shows a view looking into the lateral protocerebrum from its confluence with the optic lobes, its medial axis indicated by the black arrow and the rostral axis by the white arrow pointing upwards. Confocal levels are indicated as well as the two gyri (Ca1Gy1, Ca1Gy2) associated with the Ca1 column and the globuli cell tracts to Ca1 and Ca2 from the globuli cell cluster (gc). Other abbreviations: gct, globuli cell tract; pds, pedestal of the reniform body; Gy, gyrus. Scale bars, A-E, G, H, 10μm; C and 3–D reconstruction, 100μm.

536 Fields of 5HT- and TH-immunoreactive dendrites extend across columns. Here we show
537 fields relating to column 1 from calyx 1 that provide clear resolution of their arrangements from
538 the calycal origin to the interface with gyri (*Figure 8*). Fields are arranged at specific levels
539 along the column and they intersect different domains across the column, as occurs across the
540 parallel subdivision of the columns (lobes) of mushroom bodies in *Drosophila* and other insects
541 (Nässel and Elekes 1992; Liu et al., 2012; Aso et al., 2014a; Hamanaka, 2016; Tedjakumala et
542 al., 2017). The first of these fields occurs at the origin of the column from the calyx (*Figure*
543 *8A,B*) above where the neat orthogonal arrangements seen at deeper levels give way to the first
544 appearance of looser arrangements, including parallel fibers (*Figure 8C,F*). Anti-5HT- and anti-
545 TH-immunoreactive fields are clearly segregated (*Figure 8A and D*) at or near the column origin
546 but begin to overlap at more rostral levels closer to the gyri, at locations where osmium-ethyl
547 gallate preparations show the columns branching, with tributaries extending to overlying gyri. At
548 those levels, immunoreactive processes appear to spread laterally into the gyri themselves
549 (*Figure 8G,H*).
550
551 **6. Organization of gyriform neuropils**
552 Five distinct gyri comprise the outer layer of the RLPR (*Figure 9A*). But only four gyri are
553 associated with the two calyces. A fifth proximal gyrus situated near the entry of the eyestalk
554 nerve is notable for its neuronal organization distinguishing it as entirely separate from the
555 mushroom body (*Figure 9A,F*).
556 Mass impregnations demonstrate at this outer level of the lateral protocerebrum large
557 numbers of efferent neurons and their dendritic processes, many of which originate from clusters
558 of loosely arranged patches of perikarya that extend over the outer surface of the lateral
559 protocerebrum (*Figure 9 – figure supplement 1*). Although stochastically impregnated, the
560 abundance and variety of these neurons suggests the gyri contain dense arrangements of efferent
561 (output) and local interneurons (*Figure 9- figure supplement 1D-I*). Golgi impregnations reveal
562 swathes of axons extending across the gyri, suggesting lateral interactions amongst them.
563 Oblique palisades of dendritic trees, which have branching patterns peculiarly reminiscent of
564 vertebrate pyramidal cells (*Figure 9B*), send axons to fascicles that extend to the midbrain via
565 the eyestalk nerve.

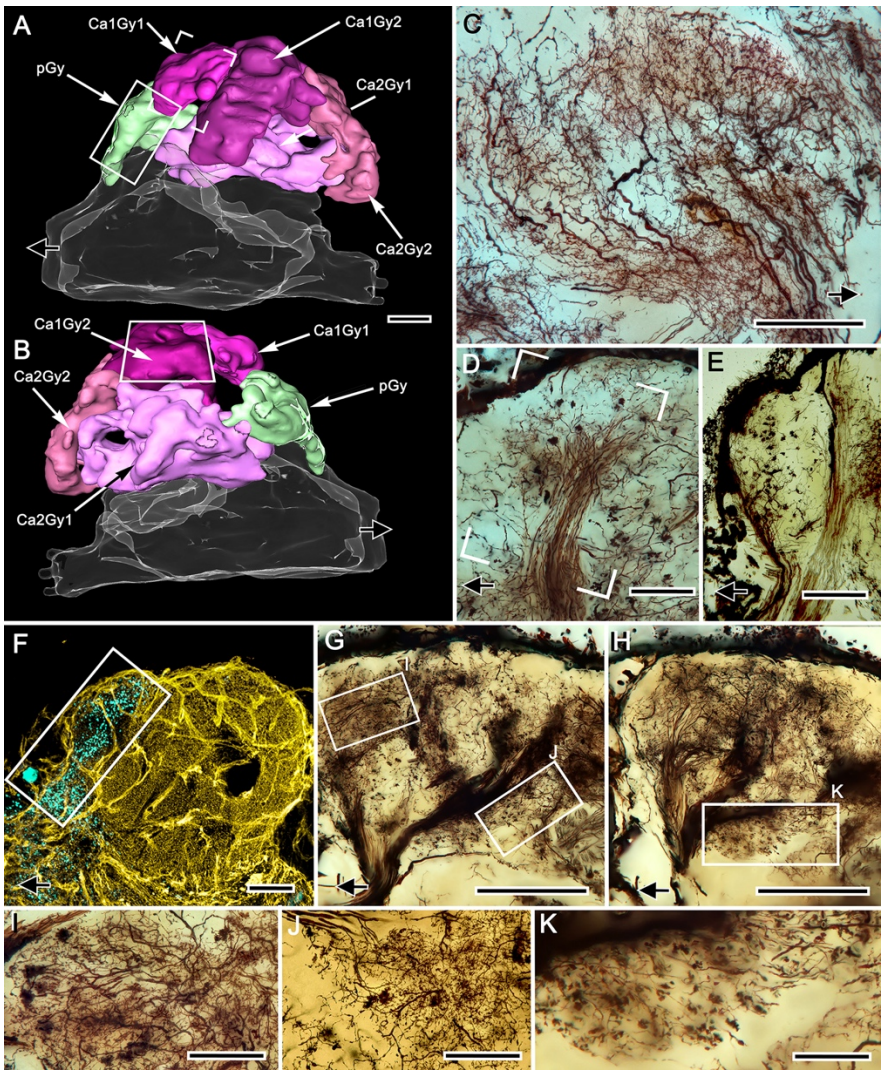

Figure 9. Gyriform neuropils: afferent and efferent organization. (**A, B**). Amira-generated 3–D reconstructions of the gyri and their calyces. Black arrows indicate the direction of the eyestalk nerve; likewise in panels C–H. (**C**) Ensemble of efferent dendrites in gyrus 2 associated with calyx 1 (Ca1Gy2). The represented area is boxed in panel B. (**D**) Afferent tributary from the antennoglomerular tract (olfactory projection neurons) suppling gyrus Ca1Gy1 neuropil (open rectangle in panel A). (**E**) Smooth oval presynaptic specializations denote the terminals of another antennoglomerular tributary that exclusively supplies the most proximal gyrus (pGY, rectangle in panel A), which has no obvious connection to the mushroom body. (**F**) Double-labelling with anti–GAD (yellow) and anti–allatostatin (cyan) of the lateral protocerebrum resolves allatostatin immunoreactivity in the proximal gyrus (rectangle in A and F), which shows little to no GAD immunoreactivity. (**G, H**) Stacked z-axis projections of Golgi-impregnated tracts, imaged through two successive 50-μm sections showing massive supply by afferent neurons. These reach levels of the lateral protocerebrum that include those at and well beneath the gyriform layer (box I, panel G), including levels of the calyces (box J in panel G and box K in panel H). Notably, many efferent neurons relaying information from gyri (panel H) send their downstream axons from the lateral protocerebrum into these tracts. (**I-K**) Enlargements from regions indicated in G, H, but at sample thicknesses of less than 20 μm to isolate details obscured in flattened optical sections . Scale bars, A–C, F–H, 100μm; D,E, 50μm; I–K, 50μm.

Figure 9 —— figure supplement 1. Perikaryal distributions and gyri neurons

586 Like deeper levels of the lateral protocerebrum, gyri comprising this superficial level of
587 the lateral protocecerum are supplied by terminals of afferent neurons, the axons of which radiate
588 out from the eyestalk nerve. Many of these terminals are identified as originating from discrete
589 fascicles that comprise the antennal globular tract, denoting not only their identity as axons of
590 projection neurons from the olfactory lobes but suggesting that different classes of projection
591 neurons comprise different fascicles (*Figure 9D,E*). The terminals of projection neurons are
592 denoted by their swollen boutons, the different morphologies of which are distinctive. For
593 example, terminals spreading out over the surface of gyrus 1, belonging to calyx 1, have rough
594 ball-shaped profiles that are distinct from larger smooth boutons from extremely slender axons
595 supplying the fifth proximal gyrus (pGy in *Figure 9A,B,E*). That gyrus's large allatostatin-
596 immunoreactive processes and the paucity, even absence, of GAD-immunoreactive networks
597 suggests its complete independence from the mushroom body's organization (*Figure 9F*). Nor,
598 as shown by osmium-ethyl gallate, is this gyrus associated with any of the calyces' outward
599 extensions.
600 In addition to axons extending from the eyestalk nerve providing afferents to superficial
601 levels in the gyri, all levels in the rostral protocerebrum receive an abundant supply of terminals,
602 including many penetrating to deep levels of the calyces (*Figure 9G-K*). Again, it is worth
603 bearing in mind when viewing the images in Figure 9G, H that Golgi impregnations likely reveal
604 not more than a few percent of the constituent neurons providing these already dense
605 arrangements of incoming fiber tracts.
606
607 **7. Transitions to gyri**
608 We have shown that four gyri overlie two large columns, each extending from one of the two
609 calyces, as do occasional smaller finger-like extensions. Osmium-ethyl gallate demonstrates that
610 the columns bifurcate close to the gyri (*Figure 1A, 2D,E*), a feature also resolved in serial
611 reduced-silver-stained sections (*Figure 7 - figure supplement 1A-H*). However, neither method
612 allows the identification of a clear inner margin of a gyrus or an obvious termination of the
613 column. Here we consider neural arrangements that denote the ambiguity of the interface
614 between the mushroom body's columns and their corresponding gyri .
615

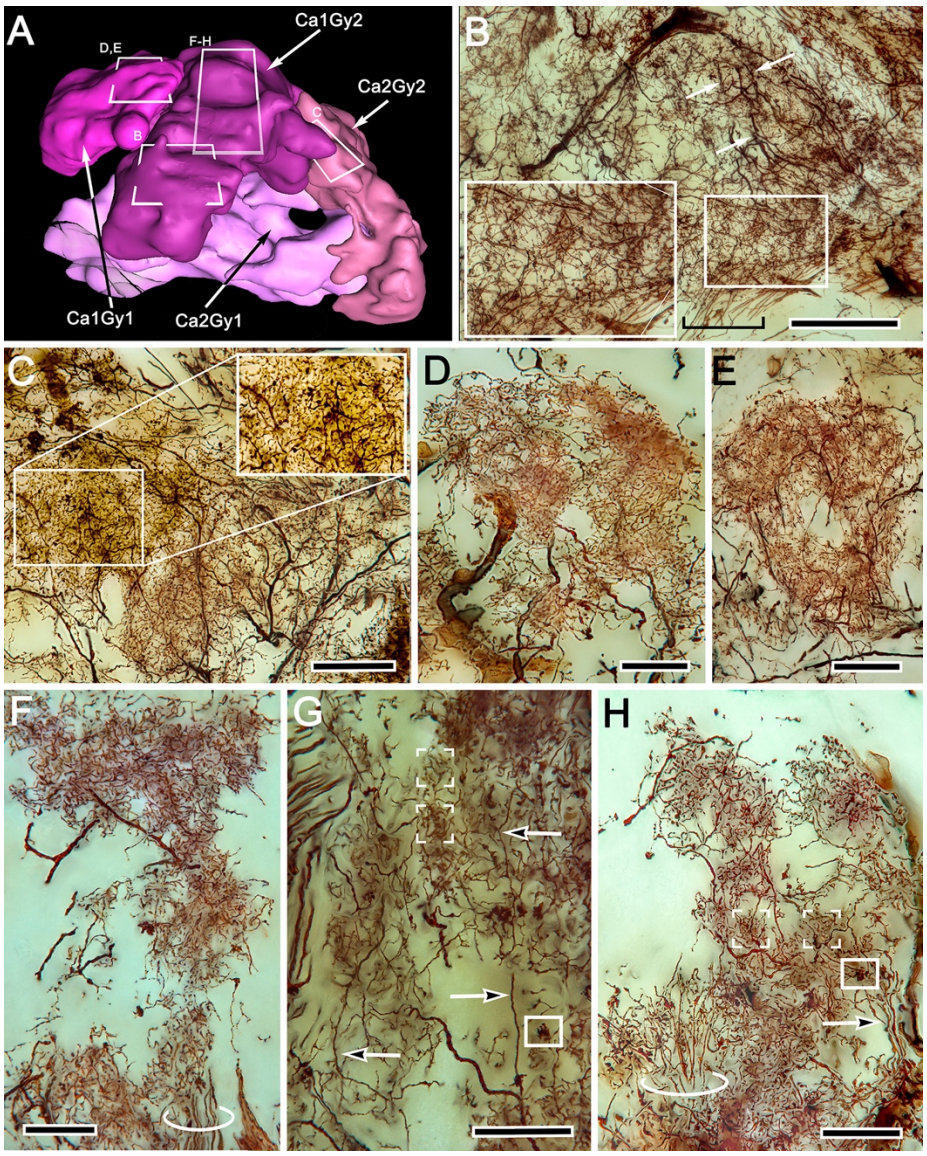

Figure 10. Gyrus neuropils: local circuit neurons. (**A**) 3-D reconstruction of gyri associated with calyx 1 and 2, showing approximate locations of networks shown in B–H. (**B**) Dense network supplied by ascending processes (boxed area is enlarged on left), ascribed to Ca1Gy2 derived from column 1. Dendrites of an efferent neuron (arrows) spread through this layer. (**C**) Efferent dendrites overlap a broad field of dense terminal specializations. Gnarled bouton-like specializations (boxed and enlarged on right) show that terminals from the eyestalk nerve enter this level. (**D-H**) Dense and elaborately branched elements interpreted as local interneurons (D, E) and intrinsic elements of the column (F-H). Ascending processes (circled in F,H and arrowed in G,H) are further evidence of local circuits. Dense groups of converging processes (box brackets in G,H) correspond in size to afferent boutons (boxed in G,H). Scale bars, B, C, 100μm: D-H, 50μm.

Figure 10 —— figure supplement 1. Column-gyrus interface organization**.**

Tangential sections across the gyri demonstrate novel and as yet puzzling aspects of their composition (*Figure 10A,B*). One is the presence of dendritic trees, as in Figure 10B, here

632 represented by a single impregnated neuron, the axon of which groups with others extending to
633 the lateral protocerebral root of the eyestalk nerve. The dendrites are seen overlapping with
634 elaborate networks of finely branching processes that terminate in small bead-like swellings
635 suggestive of presynaptic specializations. This network (*Figure 10B*) derives from extremely thin
636 processes that ascend into the gyrus from outward extensions of the calyx (bracketed in *Figure*
637 *10B*). Further examples (*Figure 10C*) show that the dendrites of a gyrus's efferent neurons
638 overlap other arrangements of putative ascending presynaptic fields. In this example, the fields
639 do not appear to be part of an intervening synaptic network but instead their disposition with the
640 efferent dendritic trees suggests that they likely terminate there (*Figure 9C*). In addition, highly
641 restricted systems of mixed spiny and beaded arborizations suggest local anaxonal neurons that
642 may provide synaptic interfaces between such terminal systems arising from the columns and the
643 dendrites of gyral efferent neurons (*Figure 10D,E*). Evidence that arborizations predominantly
644 equipped with presynaptic specializations likely originate from the calyces is indicated by
645 densely packed elements situated distally in the columns. These are equipped with short digiform
646 specializations arranged as small basket-like receptacles that clasp afferent terminals of unknown
647 origin (*Figure 10F-H*).
648 The rare Golgi impregnation that resolves one of the columns as a recognizable ensemble
649 of heterogeneous elements within the column's boundaries also demonstrates that its terminus is
650 "open," meaning contiguous with the gyral neuropil into which some of its fibers project (*Figure*
651 *7- figure supplement 1A; Figure 10 – figure supplement 1A*). Also fortuitous are preparations
652 that demonstrate the terminus of a column coinciding with bundled endings from the
653 antennoglomerular tract. Such a preparation (*Figure 10 supplement 1B*), also shows that the
654 terminus of the column is open to gyral neuropil around it and that processes extend from the
655 column into the gyrus. Combined labelling with anti-synapsin and actin at the terminus of the
656 column (*Figure 10 - figure supplement 1C*) further indicates that sizes and densities of sites
657 indicating synaptic convergence differ systematically across it. The flanking gyral neuropils also
658 betray substantial variation in synaptic densities. Inputs to the gyri do not, however, derive solely
659 from calycal columns and afferents from the antennoglomerular tract. Reduced silver shows that
660 tracts from caudal neuropil associated with the optic lobe extend rostrally to the superficial levels
661 of a gyrus (*Figure 10 - figure supplement 1D*), yet another indication of the complexity of
662 organization and its multimodal nature even at the most distal level of the mushroom body. The
663 possible significance of this is considered below in the Discussion.

664 **8. The reniform body**
665 We have shown that the lateral protocerebrum is divided into a rostral and caudal part (RLPR
666 and CLPR) , the former containing the paired mushroom bodies. The mushroom bodies are not,
667 however, the sole components of the RLPR. The pGy gyrus nearest to the RLPR's junction with
668 the eyestalk nerve is distinct and probably to some degree functionally separate from gyri
669 associated with the mushroom bodies (*Figure 9F*). In addition, there is another prominent system
670 of circumscribed neuropils situated close to the lateral border of the RLPR, arising from a dorsal
671 group of relatively small perikarya almost adjacent to the optic lobes. These neuropils comprise
672 the reniform body, a center identified in stomatopods by Bellonci (Bellonci, 1882), who
673 distinguished it from the very prominent mushroom bodies in that taxon. The same center has
674 been described in detail in the stomatopods *Neogonodactylus oerstedii*, *Gonodactylus smithii*,
675 and *G. chiragra*, and the carideans *Lebbeus groenlandicus* and *Alpheus bellulus.* In all these
676 species the reniform body adopts the same morphology: a densely populated bundle of axons,
677 referred to as the pedestal extends from the dorsal surface of the RLPR to its ventral surface,
678 providing four discrete neuropils called the initial (dorsal), lateral, and the ventrally situated
679 proximal and distal zones (Wolff et al., 2017; Thoen et al., 2019; Sayre and Strausfeld, 2019;
680 Strausfeld et al., 2020). In all of the cited taxa, the reniform body is situated between the
681 columnar mushroom body and the lobula.
682 Precisely the same placement is observed in the varunid lateral protocerebrum (*Figure*
683 *11*). The reniform body occupies a location lateral to the ensembles of neurons that constitute the
684 mushroom body gyri (*Figures 1,11*). Reconstructed from serial osmium-ethyl gallate sections,
685 the reniform body's pedestal lies immediately above, i.e., rostral to, the two tracts of neurites
686 from the globuli cell cluster (the globuli cell tract) that provide intrinsic neurons to the
687 mushroom body calyces (*Figure 11 C*). In *H. nudus*, the reniform body pedestal extends from a
688 mass of cell bodies at the dorsal surface and extends almost to the lateral protocerebrum's ventral
689 surface, bifurcating into two main tributaries about half way along its length (Figure 11 F). These
690 give rise to the lateral, distal and proximal zones, each zone composed of substantial volumes of
691 arborizations (*Figure 11 D*). The reniform body is thus entirely distinct from the mushroom
692 bodies, and is situated distally with respect to their centrally disposed calyces (*Figure 11 E*). The
693 reniform body's thick pedestal, albeit columnar in form, is distinct from a mushroom body
694 column in that its constituent axons are naked; lacking spines or other specializations that define
695 a mushroom body. The reniform body's four zones of branching collaterals contribute to

696 structures reminiscent of microglomeruli. However, they are of larger girth and synapsin-actin
697 labelling shows them to have significantly fewer converging presynaptic elements than a calycal
698 microglomerulus (*Figure 10, figure supplement 1D,E*). Despite these clear differences the
699 reniform body is strongly immunoreactive to anti-DC0 showing that it also is a learning and
700 memory center as demonstrated by Maza et al. (*Maza et al., 2016*).

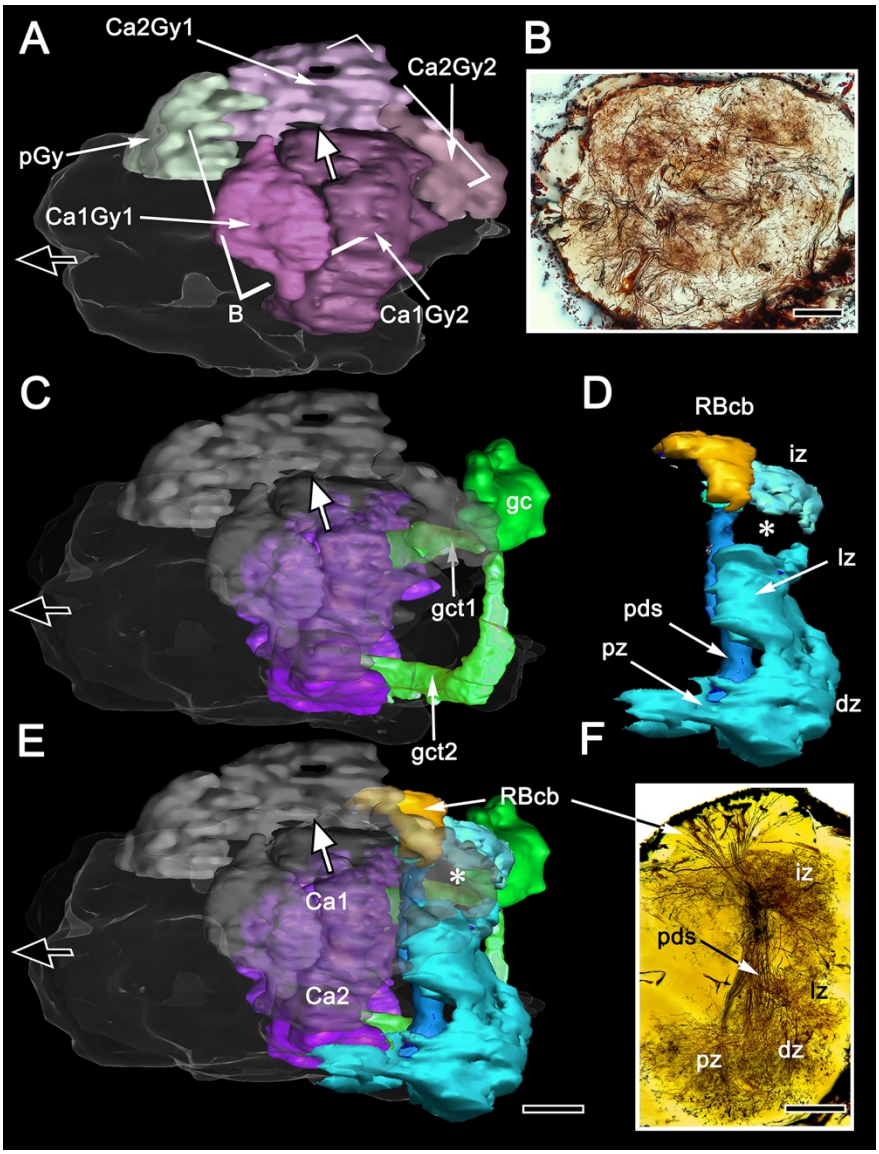

701

702 **Figure 11. Disposition of the reniform body.** (**A**) 3-D reconstruction of gyri from osmium-ethyl gallate
703 specimens identifies their 2:1 relationship with columns and their total volume, which can be compared to
704 the distribution of gyrus neurons resolved by Golgi impregnations (**B,** level indicated in A). The Golgi method
705 impregnates a fraction of the constituent neurons, the fields of which are mostly constrained to a gyrus.
706 Here impregnated neurons are viewed through the LPR's rostral surface. In panel A (and panels C E) the
707 black arrow indicates the medial axis, the white arrow the rostral axis. (**C**) The globuli cell cluster (gc)
708 provides two globuli cell tracts (gct1, gct2) to the two mushroom body calyces Ca1, Ca2. The lateral lobe
709 of gyrus 2 associated with calyx 2 (indicated by the asterisk in panel E) reaches out distally and fills a gap

710 (asterisk in D) between two processes (the intermediate and lateral zones, iz and lz) originating from the
711 reniform body's pedestal (pds). (**D**) The reniform body pedestal is a dense fiber bundle originating from a
712 dorsal cluster of small cell bodies (RBcb) on the distal flank of the RLPR. The pedestal's ventrally dividing
713 branches, shown Golgi-impregnated in panel **F**, provide the dorsal and proximal zones (dz, pz). (**E)**
714 Combined volumes in A,C, and D demonstrating the position and modest dimensions of the reniform body
715 relative to the mushroom bodies, comprising the calyces (Ca1, Ca2) and their columns and associated gyri.
716 Scale bars, A-C, B, F, 100μm.
717 **Figure 11 —— figure supplement 1**. Comparison of synaptic densities associated with the calyces and
718 reniform body.
719

720 ## Discussion

721 **Unique organization of the varunid mushroom body.** Studies by Hanström in the 1920s and
722 1930s on the brains of malacostracan crustaceans concluded that mushroom bodies equipped
723 with calyces and columns (lobes), as they are in insects and mantis shrimps (Bellonci, 1882),
724 have been reduced in decapods to columnless centers lying immediately beneath the rostral
725 surface of the lateral protocerebrum. Recent comparisons of the brains of reptantian decapods
726 have confirmed that its lineages share the evolutionary trend of reduction and loss of the
727 mushroom body column (Strausfeld and Sayre, 2019). Those mushroom bodies nevertheless
728 retain most elements of ancestral networks: diffusely arranged in Axiidea, Astacidea, Achelata
729 (Strausfeld and Sayre, 2019), but precisely stratified in terrestrial and marine Anomura, (hermit
730 crabs: Harzsch and Hansson, 2008; Wolff et al., 2012; Strausfeld and Sayre, 2019).
731 Ocypodidae (fiddler crabs) and Varunidae (shore crabs), two lineages of Brachyura (true
732 crabs) do not conform to this trend. As demonstrated previously and again here, large DC0-
733 positive domains cover much of the varunid lateral protocerebrum, suggesting relatively
734 enormous (for an arthropod) learning and memory neuropils (Strausfeld et al., 2020). The
735 proposition that the reniform body is the crab's mushroom body (Maza et al., 2016, 2020) is
736 refuted by Golgi impregnations and 3-D reconstructions of the lateral protocerebrum
737 demonstrating the reniform body as entirely distinct from the huge DC0-positive mushroom
738 body adjacent to it (*Figure 11*).
739 Similarity, conjunction, and congruence are established criteria for assessing phenotypic
740 homology (Patterson, 1988). In all the lineages where reniform bodies have been identified these
741 criteria exclude it as mushroom body homologue. That the brachyuran mushroom body has until
742 now remained unrecognized can be attributed to its hiding in plain sight as an unexpected and
743 radical reorganization. Even its population of conservatively estimated 22,000 densely packed
744 globuli cells is not where it would be expected to be. Based on observations of other

745 pancrustaceans, globuli cells are clustered over the rostral surface of the lateral protocerebrum,
746 close to where it join the eyestalk nerve (see Sayre and Strausfeld, 2019). Amplifying this
747 distinction is that the entire mushroom body is inverted such that its two voluminous calyces are
748 deeply buried in the rostral domain of the lateral protocerebrum where they receive inputs from
749 the deutocerebrum's olfactory lobes and the protocerebrum's optic lobes.
750 We show here that each calyx gives rise to a large column extending outwards and
751 merging with broad overlying gyri. The gyri are pillowed into folds and sulci thus forming a
752 cortex-like architecture. This system receives additional afferent supply and gives rise to
753 pyramidal-like ensembles of efferent neurons, the axons of which extend to the eyestalk nerve.
754 Throughout this massive structure, the mushroom body and its gyri are strongly immunoreactive
755 to antibodies raised against DC0.
756 Although the crab mushroom body appears vastly different from the right-way-up
757 "traditional" insect or stomatopod homologue (Figure 12), it nevertheless shares with them their
758 defining traits. For example, intrinsic neurons originating from globuli cells contribute to the
759 brachyuran calyces and columns as do the Kenyon cells of an insect mushroom body. As in
760 stomatopods, shrimps, and insects, the axon-like processes of intrinsic cells are clustered in their
761 respective fascicles, as they are in any one of the longitudinal divisions of the insect mushroom
762 body columns, where short intermingling collaterals can provide orthogonal connectivity
763 (Strausfeld et al. 2005; Sjöholm et al., 2005; Tanaka et al., 2008). Other longitudinal divisions of
764 the varunid mushroom body column are populated by intrinsic processes that interweave to
765 provide rectilinearity, as they do in one of the two mushroom body columns of the shrimp
766 *Lebbeus groenlandicus* (Sayre and Strausfeld, 2019), or in the stratified dome-like mushroom
767 body of hermit crabs (Wolff et al., 2015). We show here that true crabs express the whole
768 panoply of intrinsic cell arrangements. These include segregated and intermingling "parallel
769 fibers" as in Stomatopoda or the core lobe (column) of *Drosophila* (Wolff et al., 2017; Strausfeld
770 et al., 2003); rectilinear networks that extend part way into a column from the calyx; dense
771 arrangements of intrinsic processes extending across the columns comparable to certain neurons
772 populating the mushroom body column in honey bees or crickets (Strausfeld 2002; Hamanaka
773 and Mizunami, 2019); and arrangements comparable to the longitudinal laminations of the
774 mushroom body lobes (columns) of Dictyoptera and Lepidoptera (Sinakevitch et al., 2001;
775 Sjöholm et al., 2005). In short, the crab mushroom body column appears to embody all known
776 arrangements across Pancrustacea. If each arrangement of a specific type of intrinsic neurons

777 represents a distinct computational property, as suggested from studies of honeybees and fruit
778 flies (Traniello et al., 2019; Perisse et al., 2016), then the crab would appear to be singularly
779 well-equipped. The same applies to its calycal arrangements, which in *H. nudus* are elaborate
780 and discretely partitioned into territories denoted by different morphologies of intrinsic neurons
781 and afferents. This zonal organization corresponds to the more compact and highly ordered
782 modality-specific domains typifying hymenopteran calyces (Gronenberg 2001), and, to a lesser
783 extent, *Drosophila* calyces as well (Yagi et al., 2016; Li et al., 2020).
784 The varunid lateral protocerebrum has two calyces, each providing a massive column.
785 This doubling of the calyx has many precedents. In the stomatopod lateral protocerebrum there
786 are four adjacent columns, each associated with a distinct ensemble of globuli cells and hence a
787 calyx. That organization has been compared to the *Drosophila* mushroom body, which is a
788 composite neuropil of four hemi-mushroom bodies derived from four clonal lineages, as it is in
789 the honey bee (Wolff et al., 2017; Ito et al., 1997; Farris et al., 2004). Consequently, the
790 mushroom bodies in an insect's lateral protocerebrum are paired but completely fused. The
791 varunid has two calyces in immediate contact, but not quite fused as no intrinsic neuron extends
792 its field of processes into both. Only one calyx (CA2) appears to receive input from a tract of
793 axons carrying relays from the medulla and from the reniform body. Such an asymmetric input to
794 twin calyces is not unique: a comparable arrangement is found in the *Drosophila* mushroom
795 body, where visual inputs terminate in an "accessary calyx" attached to one side of the fused
796 calyx (Vogt et al., 2016). A similar arrangement involving visual inputs has been described from
797 the swallowtail butterfly (Kinoshita et al., 2015).
798 Of particular note is the extensive organization of GAD-immunoreactive arborizations
799 that extend into every domain of the *H. nudus* calyces. These provide dense systems of minute
800 processes, the dispositions of which would allow synaptic contact with every neuronal process
801 supplying a microglomerus. Accepting that varunid intrinsic neurons correspond to insect
802 Kenyon cells, these GAD-immunoreactive systems suggest correspondence with wide-field
803 anaxonal inhibitory neurons that extend throughout the *Drosophila* calyx ('APL neurons': Liu
804 and Davis, 2009; Amin et al., 2020). Consequently, such putatively inhibitory anaxonal neurons
805 in the crab suggest a global role in local synaptic inhibition at microglomeruli. Arrangements of
806 aminergic neurons in the calyces and columns further correspond to mushroom body input and
807 output neurons recognized in *Drosophila* (Aso et al., 2014; Owald et al., 2015). It is also notable
808 that highly localized and densely branching TH- and 5HT- immunoreactive neurons occur at

809 different levels of the crab's calyces. These correspond to similar dispositions of immunoreactive
810 neurons in the layered calyces of columnar mushroom bodies, including those of stomatopods
811 and shrimps (Wolff et al., 2017; Sayre and Strausfeld, 2019). Neurons with the same
812 immunoreactive signatures are associated with columns, from their origin at the calyces out to
813 the level of their "fuzzy" interface with gyri and also in the gyri. Their successive levels in a
814 column approximate the arrangements of output neurons from successive partitions of insect
815 mushroom bodies, as exemplified in cockroaches and *Drosophila* (Li and Strausfeld, 1998;
816 Tanaka et al., 2008; Aso et al., 2014b); and in crustaceans by the successive fields of efferent
817 neurons in the mushroom bodies of Stomatopoda, Stenopodidea and Caridea (Wolff et al., 2017;
818 Sayre and Strausfeld, 2018; Strausfeld et al., 2020).
819
820 **Is the organization of gyri an outlier, and what is its homologue in other lineages?**
821 Comparisons of the varunid brain with those of other pancrustaceans meet an impasse when
822 considering the lateral protocerebrum's system of gyri, a cortex-like feature that appears to be
823 special to Brachyura. As described above, there is no obvious terminus of a mushroom body
824 column: its efferent neurons merge with systems of local interneurons in the gyri and, with these
825 local interneurons, they extend amongst the dendrites of efferent neurons that leave the gyri. If
826 these arrangements do not correspond to organization in other pancrustaceans and mandibulates,
827 then what developmental events might have given rise to such a departure from the reptantian
828 ground pattern?
829 Three developmental studies on the malacostracan lateral protocerebrum should be noted.
830 Two demonstrate early stages of the formation of the larval lateral protocerebrum, in which there
831 is not yet evidence for morphogenetic reorganization in what will become the lateral
832 protocerebrum (Harzsch and Dawirs1996; Sintoni et al., 2007). The third demonstrates that
833 massive reorganization and new generation of neuropils can accompany late development in the
834 pelagic larva (Chan and Cronin, 2018). All of those authors have indicated that crustaceans can
835 undergo radical metamorphosis during the change from a pelagic larva to a preadult, the larval
836 stage providing pools of neural precursor cells for subsequent development. Those precursors
837 would likely contribute not only to the formation and differentiation of adult centers in the lateral
838 protocerebrum but also to any taxon-specific morphogenic rearrangements.
839 Might the relationship of the insect mushroom body with the rest of the brain suggest an
840 origin for the gyri? In insects, many of the mushroom body efferent neurons terminate in

841 neuropils of the superior medial protocerebrum (honeybee: Strausfeld, 2002; cockroach: Li and
842 Strausfeld 1997, 1999; *Drosophila*: Ito et al., 1998; Tanaka et al., 2008; Aso et al., 2014a,b).
843 This is the most rostral part of the forebrain in insects, comprising dense networks of local
844 interneurons that are interposed between the terminals of mushroom body outputs and the
845 dendrites of interneurons whose axons terminate in successive strata of the central complex's
846 fan-shaped body (Phillips-Portillo and Strausfeld, 2012). A comparable arrangement in
847 crustaceans with eyestalks requires that efferent neurons (particularly TH-immunoreactive
848 MBONs) from the mushroom bodies extend axons from that distant origin into the midbrain's
849 superior protocerebrum. These connections are suggested by silver-stained brains of *H. grapsus*
850 showing numerous axons from the eyestalk nerve directly target the medial protocerebrum. This
851 speaks against gyri being medial neuropils displaced distally.
852 One possible interpretation of the gyri is that they represent enormously expanded
853 versions of tubercles, swollen parts of a column typifying mushroom bodies of certain caridid
854 shrimps (in Stenopodidae and Thoridae: Sayre and Strausfeld 2019) and insects (Zygentoma,
855 Ephemeroptera: Farris, 2005). Tubercles of caridid (or insect) mushroom bodies are compact,
856 comprising tangled extensions of intrinsic neuron processes associated with a concentrated
857 system of TH- and 5HT-immunorecative processes intersecting that level of the column. Those
858 arrangements are absent from gyri. Although there are TH- and 5HT-immunorecative fields in
859 gyri, these do not appear to interact with intrinsic fibers in the columns. Nevertheless, that gyri
860 are as strongly DC0-immunoreactive as the calyces and columns suggests that they play crucial
861 roles in memory acquisition.
862 Far more elaborated than a tubercle, gyri comprise many morphologically distinct types
863 of neurons, including efferents of unknown antigenicity. The presence in gyri of local
864 interneurons and rectilinear networks further indicates an identity that is indirectly associated
865 with the mushroom body. A clue is suggested by other Reptantia, in which certain mushroom
866 body outputs target neuropils at deep levels of the lateral protocerebrum (Mellon et al., 1992a,b;
867 McKinzie et al., 2003). If these less well-studied neuropils became inverted, they would overlie the
868 inverted brachyuran mushroom bodies as do the gyri (Figure 12d,e). In that scenario, the
869 relationship between a mushroom body and its target neuropils is essentially the same as in other
870 reptantians, except a consequence of inversion is that those neuropils have been able to undergo
871 unparalleled lateral expansion and gyrification.

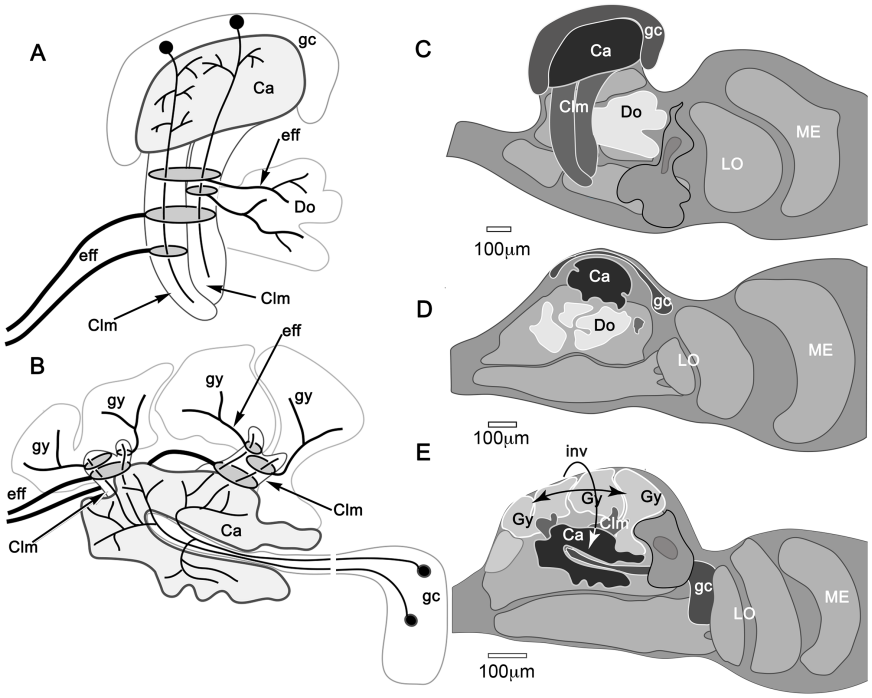

Figure 12. Mushroom body inversion and gyriform organization. (**a, b**) Schematics of corresponding neuron ground patterns. (**a**) In Stomatopoda, intrinsic neuron dendrites corresponding to the Kenyon cells of insect mushroom bodies occupy specific domains (here levels) in the calyces. Their prolongations down the columns are intersected by efferent dendritic fields, the axons of which extend to the midbrain (left) or to domains (Do) deeper in the lateral protocerebrum. (**b**) In *H. nudus*, the mushroom body is inverted. Intrinsic neuron dendrites occupy characteristic planar territories in the calyces, with rostrally projecting extensions in the columns intersected by efferent neuron dendrites. As in stomatopods (TH-MBONs), axons of some efferent neurons extend medially to the superior protocerebrum of the midbrain (not shown). Other efferents supply the gyriform neuropils overlying the lateral protocerebrum (Gy). (**c-e**) Comparisons of mushroom bodies in Malacostraca. (**c**) In the stomatopod *N. oerstedii* globuli cells cover the calyx; columns project caudally into the lateral protocerebrum neuropil. Neuropils within the lateral protocerebrum (Do) receive inputs from the lobes. (**d**) In the crayfish *Procambarus clarkia* the lobeless mushroom body lies at the lateral protocerebrum's rostral surface. Neuropils in the lateral protocecerum receiving its outputs. (**e**) In *H. nudus*, calyces are deeply buried in the lateral protocerebrum. Columns extend rostrally to an overlying gyriform neuropil with the entire arrangement indicating mushroom body inversion and lateral expansion of the rostral gyri. Abbreviations: Ca, calyx; Clm, mushroom body column; Do, domains receiving mushroom body efferents; eff, efferent neurons; gc, globuli cells; Gy, gyri; GyC, gyriform cortex; LO, lobula; ME, medulla.

The varunid mushroom body in the context of pancrustacean evolution and cognition.

The organization of characters defining mushroom bodies is phenotypically identical in stomatopods and insects (Wolff et al., 2017). The same characters have since resolved divergent homologues in all malacostracan crustaceans except Brachyura, the most recent lineage of decapod crustaceans (Wolfe et al., 2019). By identifying and describing the mushroom body of the shore crab, the present study completes the recognition of mushroom body diversification

899 and phenotypic correspondences, thereby enabling future transcriptomic verification or
900 rejection.
901 In considering the possible significance of the varunid mushroom body being larger and
902 more elaborate than that of any other pancrustacean it is relevant to consider a well-studied
903 proxy that shares with mushroom bodies circuit and genetic correspondences, as well as
904 cognitive properties. For example, it has been suggested that the cerebellum, caudal to the
905 vertebrate midbrain-hindbrain boundary, would be a fitting proxy because of comparable
906 arrangements of parallel fibers (Schürmann, 1987; Farris, 2011, Li et al., 2020). However,
907 mushroom bodies are situated rostral to the arthropod brain's deutocerebral-tritocerebral
908 boundary. A homologous location is occupied by the hippocampi, rostral to the vertebrate
909 midbrain-hindbrain boundary (Bridi et al., 2020). Mushroom bodies and hippocampi are
910 restricted, respectively, to the protocerebrum and its vertebrate homologue the telencephalon
911 (Hirth and Reichert, 1999). Neuroanatomical arrangements that are intensely immunoreactive to
912 antibodies against DC0 are shared by the hippocampus and mushroom bodies, as are at least
913 sixteen orthologous genes required for the same functions in both (Wolff and Strausfeld, 2016).
914 Gene expression profiling of early mushroom body development in *Drosophila* and of the
915 murine pallium resolve further correspondences (Tomer et al., 2010).
916 A range of behaviors supported by both the insect mushroom bodies and hippocampus
917 relate to allocentric memory, recall of place, and the use of space (Krebs et al., 1989; López et al,
918 2003; Salas et al., 2003; LaDage et al., 2009; Montgomery et al., 2016; van Djik et al., 2017).
919 Insects that are permitted explorative foraging acquire enlarged mushroom bodies compared with
920 constrained siblings, a property also pertaining to the hippocampus (Montgomery et al., 2016;
921 van Djik et al., 2017; Basil et al, 1996). As is true for mammalian and avian hippocampi
922 voluminous mushroom bodies indicate a species' reliance on spatial or social cues (Healy and
923 Krebs, 1992; Withers et al., 1993, 2008; Ott and Rogers, 2010; Molina and O'Donnell, 2007,
924 2008). Hippocampal lesions impair place memory (Day et al., 2001; Clark et al., 2005), as do
925 lesions of mushroom bodies (Mizunami et al., 1998; Buehlmann et al., 2020; Kamhi et al., 2020).
926 The volume and neuronal complexity of mushroom bodies in insects also relates to species with
927 highly developed spatial cognition (cockroaches, hymenopterans; Strausfeld et al., 2009). The
928 enormous mushroom bodies of varunid crabs suggest comparable cognitive properties relating to
929 space. Shore crabs are opportunistic generalists that live at the interface of two biotopes, marine
930 and terrestrial. They are adept at learning complex tasks (Tomsic and Romano, 2013), such as

931 maze learning (Davies et al., 2019), organizing "ad hoc" collaborative actions, establishing social
932 status (Tanner and Jackson, 2012; Kaczer et al., 2007), and memorizing acquired motor skills
933 (Hughes and O'Brien, 2001). Operant conditioning and the retention of contextual memories
934 suggest considerable intelligence (Abramson and Feinman, 1990; Pereyra et al., 1999).
935 The present description of the varunid mushroom body concludes studies establishing
936 that divergent evolution of the crustacean mushroom body maps to specific malacostracan
937 lineages. These findings offer hitherto unexplored opportunities for relating divergent cognitive
938 centers to specific ecologies and behavioral repertoires required to negotiate them.
939

940 **Materials and Methods**

941

942 **Animals.** Crabs (*Hemigrapsus nudus*), with carapace widths between 6 and 8 cms, were
943 collected from designated sites on San Juan Island, Washington, affiliated with the Friday
944 Harbor Marine Biology Laboratory (University of Washington, Seattle). Two further shipments
945 of living crabs were sent to the Strausfeld laboratory and maintained at 15˚C in tanks containing
946 seaweed continuously moistened with salt water. A total of 76 animals were used for this study
947 over an 8-year period. Twenty were used for immunohistology, 8 for osmium-ethyl gallate
948 staining, 10 for Bodian reduce silver staining and 38 for Golgi impregnations.
949

950 **Neuropil staining with osmium-ethyl gallate**. A modified ethyl gallate method (Wigglesworth
951 1957) was used to stain entire brains that were then embedded in plastic and serial sectioned.
952 These were used for Amira 3D reconstructions. After cooling to complete immobility, the
953 eyestalks were opened to expose the lateral protocerebrum. The head was then immediately
954 sliced off behind the brain and with the eyestalks immersed in 0.13 M cacodylate buffered (pH
955 6.8; Fisher Scientific, Cat#: 50-980-232) 1% paraformaldehyde with 2% glutaraldehyde
956 (Electron Microscopy Sciences, Hatfield, PA). The rest of the animal was placed in a -40˚C
957 freezer. After overnight fixation undissected tissue was soaked in buffer. The lateral protocebra
958 and midbrain were then freed of overlying exoskeleton. Next, tissue was placed for 2 h in 0.5%
959 osmium tetroxide in cacodylate buffer, continuously rocked and kept at around 4˚C in the dark.
960 After a washing in cold buffer, tissue was further well washed in distilled water while raising the
961 temperature to 20˚C. Tissue was then immersed in aqueous 0.5% ethyl gallate with constant

962 rocking. Tissue was periodically checked and when dark blue (after about 30 minutes)
963 thoroughly washed in distilled water, dehydrated, and embedded in Durcupan to be cut serially
964 into 15µm thick serial sections using a sliding microtome.
965
966 **Neuropil staining with reduced silver**. Bodian's original method (Bodian, 1936) was used, after
967 fixing tissue in an admixture consisting of 75 parts absolute ethanol, 5 parts glacial acetic acid,
968 20 parts 16% paraformaldehyde (Electron Microscopy Sciences; Cat# 16220; Hatfield, PA). As
969 for the osmium-ethyl gallate method, crabs were cooled to complete immobility, the relevant
970 parts removed, opened and fixed in AAF (70 parts absolute ethanol, 5 parts glacial acetic acid,
971 25 parts 10% E. M. grade formaldehyde). After 2-4 hours neural tissue was freed under 70%
972 ethanol, then dehydrated to absolute ethanol before clearing in terpineol. It was next soaked in
973 Xylol raising the temperature to 65˚C. Finally, tissue was transferred, via a mixture of 50:50
974 Xylol-Paraplast, into pure Paraplast (Sherwood Medical, St. Louis, MO) held at 65˚C in shallow
975 aluminum cookie dishes. After three changes, each about 3-4 minutes long, the final dish was
976 placed on icy water for the Paraplast to immediately begin to solidify. After serial sectioning at
977 10µm, sections were mounted on glycerin-albumin-subbed slides, dried, and dewaxed. Hydrated
978 material was incubated at 60˚C in 2-5% silver proteinate (Roques, Paris) for 24 h with the
979 addition of 1-4 g pure copper shot/100 ml. Afterward, sections were conventionally treated with
980 hydroquinone, gold toned, fixed, and mounted under Permount (Fisher, Springfield, NJ).
981
982 **Silver chromate (Golgi) impregnation**. Animals were anesthetized over ice. The midbrain and
983 eyestalk neural tissue was dissected free from the exoskeleton and its enveloping sheath in ice-
984 cold chromating solution comprising 1 part 25% glutaraldehyde (Electron Microscopy Sciences;
985 Cat# 16220; Hatfield, PA), 5 parts 2.5% potassium dichromate (Sigma Aldrich; Cat# 207802; St.
986 Louis, MO) with 3–12% sucrose, all dissolved in high pressure liquid chromatography (HPLC)-
987 grade distilled water (Sigma Aldrich; Ca#270733). Central brains and their detached lateral
988 protocerebra (tissues) were placed in fresh chromating solution overnight, in the dark at room
989 temperature (RT). Next, tissues were briefly rinsed (30 seconds with swirling) in 2.5% potassium
990 dichromate and transferred to an admixture of 2.5% potassium dichromate and 0.01% osmium
991 tetroxide (Electron Microscopy Sciences; Cat# 19150; Hatfield, PA) for 24 hrs. Tissues were
992 again washed in 2.5% potassium dichromate and immersed for 24 hr. in a fresh chromating

993 solution. Before silver impregnation, tissues were decanted into a polystyrene weighing dish,
994 swirled in 2.5% potassium dichromate and then gently pushed with a wooden toothpick into a
995 glass container containing fresh 0.75% silver nitrate (Electron Microscopy Sciences; Cat# 21050;
996 Hatfield, PA) in HPLC water. Tissues were twice transferred to fresh silver nitrate, then left
997 overnight in silver nitrate. Throughout, metal was not allowed to come into contact with tissue.
998 Tissues were rinsed twice in HPLC water. To achieve massive impregnation of neurons, after
999 treatment with silver nitrate tissues were washed in HPLC water and again immersed in the
1000 osmium-dichromate solution for 12hrs. and then transferred to silver nitrate as described above.
1001 After washing in HPLC water and dehydration through a four step ethanol series from 50% to
1002 100% ethanol tissues were immersed in propylene oxide (Electron Microscopy Sciences; Cat#
1003 20401; Hatfield, PA), and left for 15min. They were then subject to increasing concentrations of
1004 Durcupan embedding medium (Sigma Aldrich; Cat# 44610; St. Louis, MO) in propylene oxide
1005 during 3-5 hours. Tissues were left overnight at RT in pure liquid Durcupan and then
1006 individually oriented in the caps of BEEM capsules. These were then married to the inverted
1007 capsule cut open at its base, and were topped–up with Durcupan. Filled capsules were placed in a
1008 60°C oven for 18–24 hr. for plastic polymerization. Cooled blocks were sectioned at a thickness
1009 of 40-50µm (max) and mounted using Permount mounting medium (Fisher Scientific; Cat#
1010 SP15-100; Hampton, NH).
1011
1012 **Immunohistochemistry, antibodies**. Visualization of arrangements of immunostained neurons
1013 that further define mushroom bodies was achieved using antibodies listed in Table 1. An
1014 antibody against DC0 that recognizes the catalytic subunit of protein kinase A in D.
1015 melanogaster (Skoulakis et al., 1993) is preferentially expressed in the columnar lobes of
1016 mushroom bodies across invertebrate phyla, including members of Lophotrochozoa (Wolff &
1017 Strausfeld, 2015). Western blot assays of DC0 antibodies used on cockroach, crab, centipede,
1018 scorpion, locust, remipede, and millipede neural tissue reveal a band around 40 kDa, indicating
1019 cross-phyletic specificity of this antibody (Stemme et al., 2016; Wolff & Strausfeld, 2015).
1020 Antibodies against synapsin (Klagges et al., 1996) and α-tubulin (Thazhath et al., 2002) were
1021 used, often in conjunction with other primary antibodies, to identify dense synaptic regions and
1022 general cellular connectivity. Both antibodies likely recognize highly conserved epitope sites
1023 across Arthropoda and have been used previously in crustaceans (Andrew et al., 2012; Brauchle
1024 et al., 2009; Harzsch et al., 1997; Harzsch & Hansson, 2008; Sullivan et al., 2007). Antibodies

1025 against serotonin (5HT), glutamic acid decarboxylase (GAD), and tyrosine hydroxylase (TH)
1026 were used in this study to describe neuronal organization and in distinguishing neuropil
1027 boundaries. 5HT is an antibody that has proven to be invaluable for neuroanatomical studies
1028 across Arthropoda (Antonsen & Paul, 2001; Harzsch & Hansson, 2008; Nässel, 1988). Previous
1029 studies have used 5HT as a comparative tool for neurophylogenetic analysis (Harzsch &
1030 Waloszeck, 2000). Antibodies against GAD and TH were used to detect the enzymatic
1031 precursors of gamma aminobutyric acid (GABA) and dopamine, respectively. These two
1032 antibodies do not require the use of alternative fixation methods, making them compatible with
1033 synapsin and α-tubulin labeling, while avoiding the need to use glutaraldehyde. Comparisons of
1034 anti-GAD and anti-TH immunolabeling with that of their respective derivatives have
1035 demonstrated that these antibodies, respectively, label putative GABAergic and dopaminergic
1036 neurons (Cournil et al, 1994; Crisp et al., 2001; Stemme et al., 2016; Stern, 2009).
1037
1038 **Immunohistochemistry, application:** Methods follow those used for two recent studies on the
1039 eumalacostracan brain (Sayre & Strausfeld, 2019; Strausfeld et al., 2020). Animals were
1040 anesthetized to immobility using ice. Brains detached from nerve bundles leading to the
1041 eyestalks were first dissected free and the eyestalks were then removed. Immediately after
1042 removal, tissue was immersed in ice-cold fixative (4% paraformaldehyde in 0.1 M phosphate-
1043 buffered saline (PBS) with 3% sucrose [pH 7.4]). Midbrains and lateral protocerebra with their
1044 intact optic lobes were desheathed and left to fix overnight at 4˚C. Next, tissue was rinsed twice
1045 in PBS before being transferred to the embedding medium (5% agarose with 7% gelatin) for 1
1046 hr. at 60˚C before cooling to room temperature in plastic molds. After solidification, blocks were
1047 removed from the molds and postfixed in 4% paraformaldehyde in PBS for 1 hr. at 4˚C. The
1048 blocks were then rinsed twice in PBS and sectioned at 60 µm using a vibratome (Leica VT1000
1049 S; Leica Biosystems, Nussloch, Germany). Next, tissue sections were washed twice over a 20
1050 min. period in PBS containing 0.5% Triton-X (PBST). Tissue was subsequently blocked in
1051 PBST with 0.5% normal donkey serum (NDS; Jackson ImmunoResearch; RRID:AB_2337258)
1052 for 1hr before primary antibody incubation. Primary antibodies were added to the tissue sections
1053 at dilutions listed in Table 1. Sections were left overnight on a rotator at room temperature.
1054 Sections were next rinsed in PBST six times over the course of an hour. Donkey anti-mouse Cy3
1055 and donkey anti-rabbit Cy5 or Alexa 647 (Jackson ImmunoResearch; RRID: AB_2340813;

1056 RRID: AB_2340607; RRID: AB_2492288, respectively) IgG secondary antibodies were added
1057 to Eppendorf tubes at a concentration of 1:400 and spun for 12 min at 11,000 g. The top 900 µL
1058 of the secondary antibody solution was added to the tissue sections, which were then left to
1059 incubate overnight at room temperature on a rotator. For F-actin staining, tissue sections were
1060 left to incubate in a solution containing phalloidin conjugated to Alexa 488 (Thermo Fisher
1061 Scientific; RRID: AB_2315147) at a concentration of 1:40 in PBST for 2–3 days with constant
1062 gentle agitation following secondary antibody incubation. To label cell bodies, tissue sections
1063 were then rinsed twice in 0.1 M Tris–HCl buffer (pH 7.4) and soaked for 1 hr. in Tris–HCl
1064 buffer containing 1:2000 of the nuclear stain, Syto13 (ThermoFisher Scientific; Cat# S7575) on a
1065 rotator. Next, sections were rinsed six times in Tris–HCl over the course of 1 hr. before being
1066 mounted on slides in a medium containing 25% Mowiol (Sigma Aldrich; Cat# 81381) and 25%
1067 glycerol in PBS. Slides were covered using #1.5 coverslips (Fisher Scientific; Cat# 12-544E). To
1068 verify secondary antibody specificity, primary antibodies were omitted resulting in complete
1069 abolishment of immunolabeling. TH immunolabeling required a modified staining procedure
1070 with a shorter fixation time as well as antibody incubation in whole unsectioned tissue. Standard
1071 fixation times or sectioning the tissue prior to immunostaining resulted in poor or absent labeling
1072 as has been described previously (Cournil et al., 1994; Lange & Chan, 2008). For TH labeling,
1073 neural tissue was dissected and fixed in 4% paraformaldehyde in PBS containing 3% sucrose for
1074 30–45 min. Following fixation, neural tissue was rinsed twice in PBS, and then twice in 0.5%
1075 PBST over the course of 40 min. Tissue was then transferred to blocking buffer containing 5%
1076 NDS in 1% PBST and left to soak for 3 hr. TH primary antibody was next added to the blocking
1077 buffer at a concentration of 1:250. To assist antibody permeation, whole tissues were
1078 microwave-treated for 2 cycles of 2 min on low power (~80 W) followed by 2 min no power
1079 under a constant vacuum. Tissue was subsequently left to incubate in primary antibody solution
1080 for 2–3 days and was microwave-treated each day. After primary antibody incubation, tissue was
1081 washed with 0.5% PBST six times over the course of 2 hr. and then transferred to a solution
1082 containing 1:250 Cy3 secondary antibody. Whole mounts were left in secondary antibody
1083 overnight on a gentle shaker before being sectioned and mounted as described above. In dual
1084 labeling experiments, sectioned tissue labeled with anti-TH was then stained with an additional
1085 primary and secondary antibody also as described above.
1086

1087 **Imaging**. Confocal images were collected as Tiff files using a Zeiss Pascal 5 confocal
1088 microscope (Zeiss; Oberkochen, Germany). Image projections were made using Zeiss Zen
1089 System software. Light microscopy images were obtained using a Leitz Orthoplan microscope
1090 equipped with Plan Apochromat oil-immersion objectives (X40, X60, and X100). Series of step-
1091 focused optical sections (0.5–1.0 µm increments) were collapsed onto a single plane using
1092 Helicon Focus (Helicon Soft; Kharkov, Ukraine). Images were transferred to Adobe Photoshop
1093 (Adobe Systems, Inc; San Jose, CA) and processed using the Photoshop camera raw filter plug-
1094 in to adjust sharpness, color saturation and luminance, texture and clarity.
1095
1096 **3D-reconstruction**
1097
1098 Serial sections of osmium-ethyl gallate stained eyestalks were imaged using a brightfield Leitz
1099 Orthoplan microscope at a pixel scale of 0.5 µm x 0.5 µm. The sections were cut at a thickness
1100 of 15 µm using a rotating microtome. To account for compression and error using dry lenses
1101 because of the difference in refractive indices between glass/section and air, image sections were
1102 digitally adjusted to a voxel size of 0.5 µm x 0.5 µm x 24 µm. Additionally, to obtain a better Z-
1103 resolution, two snapshots at two focus planes were taken for each section. The resulting images
1104 were manually aligned using non-neuronal fiduciaries in the software TrakEM2 (Cardona et al.,
1105 2012).
1106 Neuropils, cell bodies, and large nerve tracts were segmented using the software Amira
1107 (Amira 2019.4; Thermo Fisher Scientific; Waltham, MA; USA). We achieved this using the
1108 Segmentation Editor, a tool which enables tracing of image data by assigning voxels to materials
1109 (i.e. user defined objects such as neuropils, cell bodies, etc.) using a paintbrush tool. Selected
1110 sections were outlined in the XY plane and interpolated across sections. Then, using the aid of
1111 the interpolated outlines, selected sections were traced in the XY, YZ and XZ planes to create a
1112 scaffold of the region of interest. The function "wrap" was then used to interpolate a 3D
1113 reconstruction of the object constrained by the scaffold. For visualization purposes, the label
1114 field containing "wrapped" labels was interpolated in Z using the "Interpolate Labels" module,
1115 adding an additional three slices for each already existing slice while maintaining the overall
1116 dimension of the reconstruction. This helped to account for the anisotropic Z-resolution (i.e.
1117 "staircase effect"). The 3D model was then visualized using the "Surface Generator" module,
1118 which created a 3D polygonal surface mesh. Images used for the figures were generated using

1119 the snapshot function. The globuli cell population was estimated on the basis of spherical

1120 globuli cells, each with the average radius of 3μm, occupying a volume of

1121 $2.5074^3 \mu m^3$ calculated from the serially reconstructed globuli cell mass.

1122

Key Resources Table				
Reagent type (species) or resource	**Designation**	**Source or reference**	**Identifiers**	**Additional information**
Biological sample	*Hemigrapsus nudus*	Friday Harbor Laboratories	N/A	n=76
Antibody	α-Tubulin (Mouse, monoclonal)	Developmental Studies Hybridoma Bank (DHSB)	CAT#: 12G10; RRID: AB_1157911	1:100
Antibody	α-Tubulin (Rabbit, polyclonal)	Abcam	CAT#: ab15246; RRID: AB_301787	1:250
Antibody	Synapsin (SYNORF1; Mouse, monoclonal)	Developmental Studies Hybridoma Bank (DHSB)	CAT#: 3C11; RRID: AB_528479	1:100
Antibody	Serotonin (5HT; Rabbit, polyclonal)	ImmunoStar	CAT#: 20080; RRID: AB_572263	1:1000
Antibody	Glutamic acid decarboxylase (GAD; Rabbit, polyclonal)	Sigma-Aldrich	CAT#: G5163; RRID: AB_477019	1:500
Antibody	Tyrosine hydroxylase (TH; Mouse, monoclonal)	ImmunoStar	CAT#: 22941; RRID: AB_572268	1:250
Antibody	Allatostatin (Ast7; Mouse, monoclonal)	Developmental Studies Hybridoma Bank (DHSB)	CAT#: 5F10; RRID:AB_528076	1:100
Antibody	DC0 (Rabbit, polyclonal)	Generous gift from Dr. Daniel Kalderon (Skoulakis et al., 1993)	RRID: AB_2314293	1:400
Antibody	AffiniPure Donkey Anti-Mouse IgG (H+L) Cy™3 (polyclonal)	Jackson ImmunoResearch	CAT#: 715-165-150; RRID: AB_2340813	1:400
Antibody	AffiniPure Donkey Anti-Rabbit IgG (H+L) Cy™5 (polyclonal)	Jackson ImmunoResearch	CAT#: 711-175-152; RRID: AB_2340607	1:400
Antibody	AffiniPure Donkey Anti-Rabbit IgG	Jackson ImmunoResearch	CAT#: 711-605-152; RRID: AB_2492288	1:400

	(H+L) Alexa Flour® 647 (polyclonal)			
Other (serum)	Normal donkey serum	Jackson ImmunoResearch	RRID: AB_2337258	N/A
Other (DNA stain)	SYTO™ 13 Green Fluorescent Nucleic Acid Stain	Thermo Fisher Scientific	CAT#: S7575	1:2000
Other (Phalloidin stain)	Alexa Fluor™ 488 Phalloidin	Thermo Fisher Scientific	CAT#: 12379; RRID: AB_2315147	1:40
Other (Chemical)	α-terpineol	Sigma-Aldrich	CAT#: 432628	N/A
Other (histology chemical)	Potassium dichromate	Sigma-Aldrich	CAT#: 207802	N/A
Other (HPLC purified water)	HPLC WATER	Sigma-Aldrich	CAT#: 270733	N/A
Other (histology chemical)	Osmium tetroxide	Electron Microscopy Sciences	CAT#: 19150	N/A
Other (histology chemical)	Ethyl gallate	Fisher Scientific	CAT#: G001625G	N/A
Other (histology chemical)	Phosphate buffer tablets	Sigma-Aldrich	CAT#:45ZE83	N/A
Other (histology chemical)	Glutaraldehyde	Electron Microscopy Sciences	CAT#: 16220	N/A
Other (histology chemical)	Paraformaldehyde	Electron Microscopy Sciences	CAT#: 15710	N/A
Other (histology chemical)	Sodium cacodylate	Electron Microscopy Sciences	CAT#: 50-980-232	N/A
Other (histology chemical)	Silver nitrate	Electron Microscopy Sciences	CAT#: 21050	N/A
Other (histology chemical)	Pure copper shot	Sigma-Aldrich	CAT#: 326488	N/A
Other (histology chemical)	Propylene oxide	Electron Microscopy Sciences	CAT#: 20401	N/A
Other (embedding resin)	Durcupan™ ACM resin (4-part component kit)	Sigma-Aldrich	CAT#: 44610	N/A
Other (embedding medium)	Paraplast Plus	Sigma-Aldrich	CA#: 76258	N/A
Other (mounting medium)	Permount mounting medium	Fisher Scientific	CAT#: SP15-100	N/A
Other (mounting medium)	Entellan	Sigma-Aldrich	CAT#: 1.07961	N/A
Software, algorithm	Photoshop CC	Adobe Inc.	N/A	N/A

Software, algorithm	Helicon Focus	Helicon Soft	N/A	N/A
Software, algorithm	Zen System Software	Zeiss	N/A	N/A
Software, algorithm	TrakEM2	Cardona et al., 2012	N/A	N/A
Software, algorithm	Amira 2019.4	Thermo Fisher	N/A	N/A
Other (microscope)	LSM 5 Pascal confocal microscope	Zeiss	N/A	N/A
Other (microscope)	Orthoplan light microscope	Leitz	N/A	N/A

References

Abramson CI, Feinman RD. 1990. Lever-press conditioning in the crab. *Physiology & Behavior* **48**:267–272. DOI: 10.1016/0031-9384(90)90311-Q

Amin H, Apostolopoulou AA, Suárez-Grimalt R, Vrontou E, Lin AC. 2020. Localized inhibition in the Drosophila mushroom body. *eLife 2020*. **9**:e56954 DOI: 10.7554/eLife.56954

Andrew DR, Brown SM, Strausfeld NJ. 2012 The minute brain of the copepod *Tigriopus californicus* supports a complex ancestral ground pattern of the tetraconate cerebral nervous systems. *Journal of Comparative Neurology* **520**:3446–3470. https://doi.org/10.1002/ cne.23099

Antonsen BL, Paul DH. 2001. Serotonergic and octopaminergic systems in the squat lobster *Munida quadrispina* (Anomura, Galatheidae). *Journal of Comparative Neurology* **439**:450–468. https://doi.org/10.1002/cne.1362

Aso Y, Hattori D, Yu Y, Johnston RM, Iyer NA, Ngo TT, Dionne H, Abbott LF, Axel R, Tanimoto H, Rubin GM. 2014a. The neuronal architecture of the mushroom body provides a logic for associative learning. *eLife 2014***, 3**:e04577 DOI: 10.7554/eLife.04577

Aso Y, Sitaraman D, Ichinose T, Kaun KR, Vogt K, Belliart-Guérin G, Plac¸ ais PY, Robie AA, Yamagata N, Schnaitmann C, Rowell WJ, Johnston RM, Ngo TT, Chen N, Korff W, Nitabach MN, Heberlein U, Preat T, Branson KM, Tanimoto H, et al. 2014b. Mushroom body output neurons encode valence and guide memory-based action selection in *Drosophila*. *eLife* **3**:e04580. DOI: https://doi.org/10.7554/eLife.04580, PMID: 25535794

Basil JA, Kamil, AC, Balda RP, Fite KV. 1996. Differences in hippocampal volume among food storing corvids. *Brain Behavior and Evolution* **47**:156-–164. DOI: 10.1159/000113235

Bellonci G. 1882. Nuove ricerche Sulla struttura del ganglio ottico della Squilla mantis. *Memorie Della Accademia Delle Scienze dell'Istituto Di Bologna, Serie 4 Tomo* **3**:419–426.

Bethe A. 1897. Das Nervensystem von *Carcinus Maenas*. Ein anatomisch-physiologischer Versuch. *Archiv für mikroskopische Anatomie* **50**: 460–546; *Archiv für mikroskopische Anatomie* **51**:382–452

Bodian D. 1936. A new method for staining nerve fibers and nerve endings in mounted paraffin sections. *Anatomical Record* **65**:89–97. https://doi.org/10.1002/ar.1090650110

Brauchle M, Kiontke K, MacMenamin P, Fitch DHA, Piano F. 2009. Evolution of early embryogenesis in rhabditid nematodes. *Developmental Biology* **335**:253–262. https://doi.org/10.1016/j.ydbio.2009.07.033

Bridi JC, Ludlow ZN, Kottler B, Hartmann B, Broeck LV, Dearlove J, Göker M, Strausfeld NJ, Callaerts P, Hirth F. 2020. Ancestral regulatory mechanisms specify conserved midbrain circuitry in arthropods and vertebrates. *PNAS* **117**:19544-19555. DOI: 10.1073/pnas.1918797117

Buehlmann C, Wozniak B, Goulard R, Webb B, Graham P, Niven JE. 2020 Mushroom bodies are required for learned visual navigation, but not for innate visual behavior, in ants. *Current Biology* **23**. https://doi.org/10.1016/j.cub.2020.07.013

Cardona A, Saalfeld S, Schindelin J, Arganda-Carreras I, Preibisch S, Longair M, ... Douglas RJ. 2012. TrakEM2 software for neural circuit reconstruction. *PloS one* **7**:e38011. DOI: 10.1371/journal.pone.0038011

Clark RE, Broadbent NJ, Squire LR. 2005. Impaired remote spatial memory after hippocampal lesions despite extensive training beginning early in life. *Hippocampus* **15**:340–346. doi:10.1002/hipo.20076

Cournil I, Helluy SM, Beltz BS. 1994. Dopamine in the lobster *Homarus gammarus*. I. Comparative analysis of dopamine and tyrosine hydroxylase immunoreactivities in the nervous system of the juvenile. *Journal of Comparative Neurology* **334**:455–469. https://doi.org/10. 1002/cne.903440308

Crisp KM, Klukas KA, Gilchrist LS, Nartey AJ, Mesce KA. 2001. Distribution and development of dopamine- and octopamine synthesizing neurons in the medicinal leech. *Journal of Comparative Neurology* **442**:115–129. https://doi.org/10.1002/cne.10077

Davies R, Gagen MH, Bull JC, Pope EC. 2019. Maze learning and memory in a decapod crustacean. *Biology Letters* **1520190407**. http://doi.org/10.1098/rsbl.2019.0407

Day LB, Crews D, Wilczynski W. (2001. Effects of medial and dorsal cortex lesions on spatial memory in lizards, *Behaviour Brain Research* **118**:27–42.

Ehmer B, Gronenberg W. 2002. Segregation of visual input to the mushroom bodies in the honeybee (Apis mellifera). *Journal of Comparative Neurology* 451:362–373. doi:10.1002/cne.10355

Farris SM. 2005. Developmental organization of the mushroom bodies of *Thermobia domestica* (Zygentoma, Lepismatidae): insights into mushroom body evolution from a basal insect. *Evolution & Development* **7**:150–159. doi:10.1111/j.1525-142X.2005.05017.x

Farris SM. 2011. Are mushroom bodies cerebellum-like structures? *Arthropod Structure & Development* **40**:368-379. https://doi.org/10.1016/j.asd.2011.02.004

Farris SM, Schulmeister S. 2011. Parasitoidism, not sociality, is associated with the evolution of elaborate mushroom bodies in the brains of hymenopteran insects. *Proceedings of the Royal Society B*. **278**:940–951. http://doi.org/10.1098/rspb.2010.2161

Farris M, Strausfeld NJ. 2003. A unique mushroom body substructure common to basal cockroaches and to termites. *Journal of Comparative Neurology* **456**:305–320. doi:10.1002/cne.10517

Farris SM, Abrams AI, Strausfeld NJ. 2004. Development and morphology of Class II Kenyon cells in the mushroom bodies of the honey bee, *Apis mellifera*. *Journal of Comparative Neurology* **474**:325-339. doi:10.1002/cne.20146

Groh C, Rössler W. 2011. Comparison of microglomerular structures in the mushroom body calyx of neopteran insects. *Arthropod Structure & Development* **40**:358-367. https://doi.org/10.1016/j.asd.2010.12.002

Gronenberg W. 2001. Subdivisions of hymenopteran mushroom body calyces by their afferent supply. *The Journal of Comparative Neurology* **435**: 474-489. doi:10.1002/cne.1045

Guinot D. 2019. New hypotheses concerning the earliest brachyurans (Crustacea, Decapoda, Brachyura) *Geodiversitas* **41**:747-796. https://doi.org/10.5252/geodiversitas2019v41a22

Hamanaka Y, Mizunami M. 2019. Tyrosine hydroxylase-immunoreactive neurons in the mushroom body of the field cricket, *Gryllus bimaculatus*. *Cell Tissue Res* **376:**97–111. https://doi.org/10.1007/s00441-018-2969-9

Hamanaka Y, Minoura R, Nishino H, Miura T, Mizunami M. 2016) Dopamine- and tyrosine hydroxylase-immunoreactive neurons in the brain of the american cockroach, *Periplaneta americana*. *PLoS One* **11**:e0160531. doi: 10.1371/journal.pone.0160531

Hartnell RG. 1988. Evolution, systematics and geographical distribution. In: *Biology of the land crabs* (WW Burggren, BR McMahon, eds). Cambridge UP, Cambridge New York, Sydney. Pp. 6–54

Harzsch S, Anger K, Dawirs RR. 1997. Immunocytochemical detection of acetylated α-tubulin and *Drosophila* synapsin in the embryonic crustacean nervous system. *International Journal of Developmental Biology* **41**:477–484.

Harzsch S, Dawirs RR. 1996. Neurogenesis in the developing crab brain: Postembryonic generation of neurons persists beyond metamorphosis. *Journal of Neurobiology* **29**:384–398. doi:10.1002/(SICI)1097-4695(199603)29:3<384::AID-NEU9>3.0.CO;2-5

Harzsch S, Hansson BS. 2008. Brain architecture in the terrestrial hermit crab Coenobita clypeatus(Anomura, Coenobitidae), a crustacean with a good aerial sense of smell. *BMC Neuroscience* **9**:58. DOI: https://doi.org/ 10.1186/1471-2202-9-58

Harzsch S, Waloszeck D. 2000. Serotonin-immunoreactive neurons in the ventral nerve cord of Crustacea: A character to study aspects of arthropod phylogeny. *Arthropod Structure & Development* **29**:307–322. https://doi.org/10.1016/S1467-8039(01)00015-9

Healy SD Krebs JR. 1992. Food storing and the hippocampus in corvids: amount and volume are correlated. *Proceedings of the Royal Society of London B* **248**:241–245 http://doi.org/10.1098/rspb.1992.0068

Heuer CM, Lössel R. 2009. Three-dimensional reconstruction of mushroom body neuropils in the polychaete species *Nereis diversicolor* and *Harmothoe areolata* (Phyllodocida, Annelida). *Zoomorphology* **128**:219–226.DOI 10.1007/s00435-008-0063-7

Hirth F, Reichert H. 1999, Conserved genetic programs in insect and mammalian brain development. *Bioessays* **21**:677–684. https://doi.org/10.1002/(SICI)1521-1878(199908)21:8<677::AID-BIES7>3.0.CO;2-8

Hughes RN, O'Brien N.. 2001. Shore crabs are able to transfer learned handling skills to novel prey. Animal Behavior 61:711–714. DOI: 10.1006/anbe.2000.1640

Ito K, Awano W, Suzuki K, Hiromi Y, Yamamoto D. 1997. The *Drosophila* mushroom body is a quadruple structure of clonal units each of which contains a virtually identical set of neurones and glial cells. *Development* **124**:761–771. PMID: 9043058

Ito K, Suzuki K, Estes P, Ramaswami M, Yamamoto D, Strausfeld NJ. 1998. The organization of extrinsic neurons and their implications in the functional roles of the mushroom bodies in *Drosophila melanogaster* Meigen. *Learning & Memory* **5**:52–77. PMID: 10454372

Ito K, Shinomiya K, Ito M, Armstrong JD, Boyan G, Hartenstein V, Harzsch S, Heisenberg M, Homberg U, Jenett A, Keshishian H, Restifo LL, Rössler W, Simpson JH, Strausfeld NJ, Strauss R, Vosshall LB, Insect Brain Name Working Group. 2014. A systematic nomenclature for the insect brain. *Neuron* **81**:755–765. DOI: https://doi.org/10.1016/j.neuron.2013.12.017, PMID: 24559671

Jacob PF, Waddell S. 2020. Spaced training forms complementary long-term memories of opposite valence in *Drosophila*. *Neuron* **106**:977-991.e4. https://doi.org/10.1016/j.neuron.2020.03.013

Jacoby CA. 1981. Behavior of the Purple Shore Crab *Hemigrapsus nudus* Dana, 1851. *Journal of Crustacean Biology* **1**:531–544. https://doi.org/10.2307/1548130

Kaczer L, Pedetta S, Maldonado H. 2007. Aggressiveness and memory: Subordinate crabs present higher memory ability than dominants after an agonistic experience. *Neurobiology of Learning and Memory* **87**:140–148. DOI: 10.1016/j.nlm.2006.08.002

Kalderon D, Rubin GM. 1988. Isolation and characterization of Drosophila cAMP-dependent protein kinase genes. *Genes & Development* **2**:1539–1556. DOI: https://doi.org/10.1101/gad.2.12a.1539, PMID: 3215511

Kamhi JF, Barron AB, Narendra A. (2020). Vertical lobes of the mushroom bodies are essential for view-based navigation in Australian bull ants. *Current Biology* **23**: https://doi.org/10.1016/j.cub.2020.06.030.

Kanzaki R, Arbas EA, Strausfeld NJ, Hildebrand JG. 1989. Physiology and morphology of projection neurons in the antennal lobe of the male moth *Manduca sexta*. *Journal of Comparative Physiology A* **165**:427–453.

Kinoshita M. Shimohigasshi M, Tominaga Y, Arikawa K., Homberg, U. 2015. Topographically distinct visual and olfactory inputs to the mushroom body in the Swallowtail butterfly, *Papilio xuthus*. *Journal of Comparative Neurology* **523**:162–182. doi:10.1002/cne.23674

Klagges BR, Heimbeck G, Godenschwege TA, Hofbauer A, Pflugfelder GO, Reifegerste R. et al. 1996. Invertebrate synapsins: A single gene codes for several isoforms in *Drosophila*. *Journal of Neuroscience* **16**:3154–3165. https://doi.org/10.1523/JNEUROSCI.16-10-03154.1996

Krebs J, Sherry DF, Healy SD, Perry VH, Vaccarino AL. 1989. Hippocampal specialization of food-storing birds (passerines/memory). *PNAS* **86:**1388–1392.

LaDage LD, Riggs BJ, Sinervo B ,Pravosudov VV. 2009. Dorsal cortex volume in male side-blotched lizards, *Uta stansburiana*, is associated with different space use strategies. *Animal behavior* **78**:91-96. DOI: 10.1016/j.anbehav.2009.03.020

Lange AB, Chan K. 2008. Dopaminergic control of foregut contractions in *Locusta migratoria*. *Journal of Insect Physiology* **54**:222–230. https://doi.org/10.1016/j.jinsphys.2007.09.005

Lee SY. 2015. *Ecology of Brachyura*. In: Treatise on Zoology - Anatomy, Taxonomy, Biology. *The Crustacea* **9C**:469–541.DOI: https://doi.org/10.1163/9789004190832_011

Leitch B, Laurent G. 1996. GABAergic synapses in the antennal lobe and mushroom body of the locust olfactory system. *Journal of Comparative Neurology* **372**:487–514. doi:10.1002/(SICI)1096-9861(19960902)372:4<487::AID-CNE1>3.0.CO;2-0

Li F, Lindsey J, Marin EC, Otto N, Dreher M, Dempsey G, et al. (2020). The connectome of the adult *Drosophila* mushroom body: implications for function. BioRxiv. doi: https://doi.org/10.1101/2020.08.29.273276

Li Y, Strausfeld NJ. 1997. Morphology and sensory modality of mushroom body extrinsic neurons in the brain of the cockroach, *Periplaneta americana.The Journal of Comparative Neurology* **387**: 631-650. doi:10.1002/(SICI)1096-9861(19971103)387:4<631::AID-CNE9>3.0.CO;2-3

Li Y, Strausfeld NJ. 1999. Multimodal efferent and recurrent neurons in the medial lobes of cockroach mushroom bodies. *The Journal of Comparative Neurology* **409**:647–663. DOI: https://doi.org/10.1002/(SICI)1096-9861

Li J, Mahoney BD, Jacob MS, Caron SJC. 2020. Visual input into the *Drosophila melanogaster* mushroom body**.** *Cell Reports* **30:** https://doi.org/10.1016/j.celrep.2020.108138

Lin C, Strausfeld NJ. 2012. Visual inputs to the mushroom body calyces of the whirligig

beetle *Dineutus sublineatus*: Modality switching in an insect. *The Journal of Comparative Neurology* **520**:2562-2574. doi:10.1002/cne.23092

Lin C, Cronin TW. 2018. Two visual systems in one eyestalk: The unusual optic lobe metamorphosis in the stomatopod *Alima pacifica*. *Developmental Neurobiology* **78**: 3–14. https://doi.org/10.1002/dneu.22550

Liu X, Davis R. 2009. The GABAergic anterior paired lateral neuron suppresses and is suppressed by olfactory learning. *Nature Neuroscencei* **12,** 53–59 (2009). https://doi.org/10.1038/nn.2235

Liu C, Plaçais P, Yamagata N, Pfeiffer BD, Aso Y, et al. .2012. A subset of dopamine neurons signals reward for odour memory in *Drosophila*. *Nature* **488**:512–516. https://doi.org/10.1038/nature11304

López JC, Vargas JP, Gómez Y, Salas C. (2003) Spatial and non-spatial learning in turtles: the role of medial cortex, *Behaviour Brain Research* **143**:109–120.

Maza FJ, Sztarker J, Shkedy A, Peszano VN, Locatelli FF, Delorenzi A. 2016. Context-dependent memory traces in the crab's mushroom bodies: Functional support for a common origin of high-order memory centers. *Proceedings of the National Academy of Science USA* **113**:E7957–E7965. DOI: https://doi.org/10.1073/pnas.1612418113, PMID: 27856766

Maza FJ, Sztarker J, Cozzarin ME, Lepore MG, Delorenzi A. 2020. A crabs' high-order brain center resolved as a mushroom body-like structure. *The Journal of Comparative Neurology*. 2020:1– 23. https://doi.org/10.1002/cne.24960

McKinzie ME, Benton JJ, Beltz BS, Mellon DF Jr. 2003. Parasol cells of the hemiellipsoid body in the crayfish Procambarus clarkii: Dendritic branching patterns and functional implications. *Journal of Comparative Neurology* **462**:168–179. https://doi.org/10.1002/cne.10716

Mellon DF Jr., Alones V, Lawrence MD. 1992a. Anatomy and fine structure of neurons in the deutocerebral projection pathway of the crayfish olfactory system. *The Journal of Comparative Neurology* **321**:93–111. doi:10.1002/cne.903210109

Mellon DF Jr., Sandeman DC, Sandeman RE. 1992b. Characterization of oscillatory olfactory interneurons in the protocerebrum of the crayfish. *Journal of Experimental Biology* **167**:5–38.

Mizunami M, Weibrecht JM, Strausfeld NJ. 1998. Mushroom bodies of the cockroach: their participation in place memory. *The Journal of Comparative Neurology* **402**:520–537.

Molina Y, O'Donnell S.. 2007. Mushroom body volume is related to social aggression and ovary development in the paperwasp *Polistes instabilis. Brain Behavoir and Evolution* **70**:137–144. (doi:10.1159/000102975).

Molina Y, O'Donnell S. 2008. Age, sex, and dominance-related mushroom body plasticity in the paper wasp *Mischocyttarus mastigophorus*. *Developmental Neurobiology* **68**:950–959. (doi:10.1002/dneu.20633).

Montgomery SH, Ott SR. 2015. Brain composition in *Godyris zavaleta*, a diurnal butterfly, reflects an increased reliance on olfactory information. *The Journal of Comparative Neurology* **523**:869–891. doi:10.1002/cne.23711

Montgomery SH, Merrill RM, Ott SR. 2016. Brain composition in *Heliconius* butterflies, posteclosion growth and experience-dependent neuropil plasticity. *The Journal of Comparative Neurology* **524**:1747–1769. DOI: https://doi. org/10.1002/cne.23993, PMID: 26918905

Modi MN, Shuai Y, Turner GC. 2020.The Drosophila mushroom body: from architecture to algorithm in a learning circuit. *Annual Review of Neuroscience* **43**:465–84. https://doi.org/10.1146/annurev-neuro-080317- 0621333

Nässel DR, Elekes K. 1992. Aminergic neurons in the brain of blowflies and Drosophila: dopamine- and tyrosine hydroxylase-immunoreactive neurons and their relationship with putative histaminergic neurons. *Cell & Tissue Research* **267**:147–167. DOI: https://doi.org/10.1007/BF00318701, PMID: 1346506

Ng PKL, Guinot D, Davie PJF. 2008. Systema brachyurorum: part I. an annotated checklist of extant brachyuran crabs of the world. *Raffles Bulletin of Zoology Supplement Series* **17**:1–286.

Okamura JY, Strausfeld NJ. 2007. Visual system of calliphorid flies: Motion- and orientation-sensitive visual interneurons supplying dorsal optic glomeruli. *Journal of Comparative Neurology* **500**:189–205. https://doi.org/10.1002/cne.21195

Owald D, Felsenberg J, Talbot CB, Das G, Perisse E, Huetteroth W, Waddell S. 2015. Activity of defined mushroom body output neurons underlies learned olfactory behavior in Drosophila. *Neuron* **86**:417–427. DOI: https://doi.org/10.1016/j.neuron.2015.03.025, PMID: 25864636

Phillips-Portillo J, Strausfeld NJ. 2012. Representation of the brain's superior protocerebrum of the flesh fly, *Neobellieria bullata*, in the central body. *Journal of Comparative Neurology* **520**:3070–3087. doi:10.1002/cne.23094

Ott SR, Rogers SM. 2010. Gregarious desert locusts have substantially larger brains with altered proportions compared with the solitarious phase. *Proceedings of the Royal Society B* **277**:3087–3096

Patel RN, Cronin TW. 2020. Mantis shrimp navigate home using celestial and idiothetic path integration. *Current Biology* **30**:1981–1987. https://doi.org/10.1016/j.cub.2020.03.023

Pereyra P, Saraco M, Maldonado H. 1999. Decreased response or alternative defensive strategies in escape: two different types of long-term memory in the crab *Chasmagnathus*. *Journal of Comparative Physiology* **A** 184:301–310. DOI: 10.1007/s003590050328

Perisse E, Yin Y, Lin AC, Lin S, Huetteroth W, Waddell S. 2013. Different Kenyon cell populations drive learned approach and avoidance in *Drosophila*. *Neuron* **79**:945-956. (doi:10.1016/J.NEURON.2013.07.045)

Salas C, Broglio C, Rodriguez F .2003. Evolution of forebrain and spatial cognition in vertebrates: conservation across diversity. *Brain, Behavior and Evolution* **62**:72–82.

Sandeman DC, Scholtz G, Sandeman RE. 1993. Brain evolution in decapod crustacea. *Journal of Experimental Zoology* **265**:112–133. DOI: https://doi.org/10.1002/jez.1402650204

Sayre ME, Strausfeld NJ. 2019. Mushroom bodies in crustaceans: Insect-like organization in the caridid shrimp *Lebbeus groenlandicus*. *Journal of Comparative Neurology* **527**:2371–2387. DOI: https://doi.org/10.1002/cne.24678

Schürmann F-W. 1987. The architecture of the mushroom bodies and related neuropils in the insect brain. In: *Arthropod Brain: Its Evolution, Development, Structure, and Functions* (ed. A.P. Gupta). John Wiley & Sons, New York. 231-264.

Schweitzer CE, Feldmann RM. 2010. The oldest Brachyura (Decapoda: Homolodromioidea: Glaessneropsoidea) known to date (Jurassic). *Journal of Crustacean Biology* **30**:251-256.

Sinakevitch I, Farris SM, Strausfeld NJ. 2001. Taurine-, aspartate- and glutamate-like immunoreactivity identifies chemically distinct subdivision of Kenyon cells in the cockroach mushroom body. *Journal of Comparative Neurology* **439**: 352–367. doi:10.1002/cne.1355

Sintoni S, Fabritius-Vilpoux K, Harzsch S. 2007. The engrailed-expressing secondary head spots in the embryonic crayfish brain: Examples for a group of homologous neurons in Crustacea and Hexapoda? *Development Genes & Evolution* **217**:791– 799. https://doi.org/10.1007/s00427-007-0189-5

Sjöholm M, Sinakevitch I, Ignell R, Strausfeld NJ, Hansson BS. 2005. Organization of Kenyon cells in subdivisions of the mushroom bodies of a lepidopteran insect. *Journal of Comparative Neurology* **491**: 290-304. doi:10.1002/cne.20698

Sjöholm M, Sinakevitch I, Strausfeld NJ, Ignell R, Hansson BS. 2006. Functional division of intrinsic neurons in the mushroom bodies of male *Spodoptera littoralis* revealed by antibodies against aspartate, taurine, FMRF-amide, Mas-allatotropin and DC0. *Arthropod Structure & Development* **35**:153-168. https://doi.org/10.1016/j.asd.2006.03.001

Skoulakis EMC, Kalderon D, Davis RL. 1993. Preferential expression in mushroom bodies of the catalytic subunit of protein kinase a and its role in learning and memory. *Neuron* **11**:197–208. https://doi. org/10.1016/0896-6273(93)90178-T

Stegner ME, Richter S. 2011. Morphology of the brain in *Hutchinsoniella macracantha* (Cephalocarida, crustacea). *Arthropod Structure & Development* **40**:221–243. DOI: https://doi.org/10.1016/j.asd.2011.04.001, PMID: 21679884

Stemme T, Iliffe TM, Bicker G. 2016. Olfactory pathway in *Xibalbanus tulumensis*: Remipedian hemiellipsoid body as homologue of hexapod mushroom body. *Cell and Tissue Research* **363**:635–648. https://doi.org/10.1007/s00441-015-2275-8

Stern M. 2009. The PM1 neurons, movement sensitive centrifugal visual brain neurons in the locust: Anatomy, physiology, and modulation by identified octopaminergic neurons. *Journal of Comparative Physiology A* **195**:123–137. https://doi.org/10.1007/s00359-008-0392-5

Strausfeld NJ. 2012. Arthropod Brains: Evolution, Functional Elegance, and Historical Significance. Boston, MA: Harvard Belknap Press.

Strausfeld NJ. 2002. Organization of the honey bee mushroom body: Representation of the calyx within the vertical and gamma lobes. *Journal of Comparative Neurology* **450**:4-33. doi:10.1002/cne.10285

Strausfeld NJ. 2020. Nomen est omen, cognitive dissonance and homology of memory centers in crustaceans and insects. *Journal of Comparative Neurology*. doi:10.1002/cne.24919

Strausfeld NJ, Li Y. 1999. Representation of the calyces in the medial and vertical lobes of cockroach mushroom bodies. *Journal of Comparative Neurology* **409**:626–646. doi:10.1002/(SICI)1096-9861(19990712)409:4<626::AID-CNE8>3.0.CO;2-B

Strausfeld NJ, Sayre ME. 2020. Mushroom bodies in Reptantia reflect a major transition in crustacean brain evolution. *Journal of Comparative Neurology* **528**:261–282. https://doi.org/10.1002/cne. 24752

Strausfeld, N. J., Wolff, G. H., & Sayre, M. E. (2020). Mushroom body evolution demonstrates homology and divergence across Pancrustacea. *eLife* **9** (e52411), 1–46. https://doi.org/10.7554/eLife. 52411

Strausfeld NJ, Sinakevitch I, Brown SM, Farris SM. 2009. Ground plan of the insect mushroom body: functional and evolutionary implications. *Journal of Comparative Neurology* **513**:265–291. DOI: https://doi.org/10.1002/cne.21948, PMID: 19152379

Strausfeld NJ, Hansen L, Li Y, Gomez RS, Ito K. 1998. Evolution, discovery, and interpretations of arthropod mushroom bodies. *Learning & Memory* **5**:11–37. (doi:10.1101/lm.5.1.11)

Strausfeld NJ, Sinakevitch I, Vilinsky, I. 2003. The mushroom bodies of *Drosophila melanogaster*: an immunocytological and Golgi study of Kenyon cell organization in the calyces and lobes. *Microscopy Research and Technique* **62**:151–169.

Sullivan JM, Benton JL, Sandeman DC, Beltz BS. 2007. Adult neurogenesis: A common strategy across diverse species. *Journal of Comparative Neurology* **500**:574–584. https://doi.org/10.1002/cne.21187

Tanaka, N.K., Tanimoto, H. and Ito, K. (2008), Neuronal assemblies of the Drosophila mushroom body. *Journal of Comparative Neurology* **508**:711–755. doi:10.1002/cne.21692

Tanner CJ, Jackson AL. 2012. Social structure emerges via the interaction between local ecology and individual behaviour. *Journal of Animal Ecology* **81**:260-267 doi: 10.1 1 1 1/j. 1 365-2656.201 1 .01879.x

Tedjakumala SSR, Rouquette J, Boizeau M-L, Mesce KA, Hotier L, Massou I, Giurfa. 2017. Tyrosine-hydroxylase characterization of dopaminergic neurons in the honey bee brain. *Frontiers in Systems Neuroscience* **11**:47. https://www.frontiersin.org/article/10.3389/fnsys.2017.00047

Thazhath R, Liu C, Gaertig J.2002. Polyglycylation domain of β-tubulin maintains axonemal architecture and affects cytokinesis in Tetrahymena. *Nature Cell Biology* **4**:256–259. https://doi.org/10. 1038/ncb764

Tomer R, Denes AS, Tessmar-Raible K, Arendt D. 2010. Profiling by image registration reveals common origin of annelid mushroom bodies and vertebrate pallium. *Cell* **142**:800–809. doi:10. 1016/j.cell.2010.07.043.

Tomsic D, Romano A. 2013. A multidisciplinary approach to learning and memory in the crab *Neohelice* (*Chasmagnathus*) *granulata*. *Handbook of Behavioral Neuroscience* **22**:337-355. https://doi.org/10.1016/B978-0-12-415823-8.00026-5

Traniello IM, Chen Z, Bagchi VA, Robinson GE. 2019. Valence of social information is encoded in different subpopulations of mushroom body Kenyon cells in the honeybee brain. *Proceedings of the Royal Society **B*** 286:20190901. http://dx.doi.org/10.1098/rspb.2019.0901

Turner GC, Bazhenov M, Laurent G. 2008. Olfactory representations by Drosophila mushroom body neurons. *Journal of Neurophysiology* **99**:734–746. https://doi.org/10.1152/jn.01283.2007

van Dijk LJA, Janz N, Schäpers A, Gamberale-Stille G, Carlsson MA. 2017. Experience-dependent mushroom body plasticity in butterflies: consequences of search complexity and host range. *Proceedings of the Royal Society B* **284**:20171594. http://dx.doi.org/10.1098/rspb.2017.1594

Vogt K, Aso Y, Hige T, Knapek S, et al. 2016. Direct neural pathways convey distinct visual information to *Drosophila* mushroom bodies. *eLife 2016* **5**:e14009 DOI: 10.7554/eLife.14009

Wigglesworth VB. 1957. The use of osmium in the fixation and staining of tissues. *Proceedings of the Royal Society B* **147**:185–199. https://doi.org/10.1098/rspb.1957.0043

Withers GS, Fahrbach SE, Robinson GE. 1993. Selective neuroanatomical plasticity and division of labour in the honeybee. *Nature* **364**:238–240. doi:10.1038/364238a0

Withers G, Day NF, Talbot EF, Dobson HEM, Wallace CS. 2008. Experience-dependent plasticity in the mushroom bodies of the solitary bee *Osmia lignaria* (Megachilidae). *Developmental Neurobiology* **68**:73–82. doi:10.1002/dneu.20574.

Wolfe JM, Breinholt JW, Crandall KA, Lemmon AR, Lemmon EM, Timm LE, Siddall ME, Bracken-Grissom HD. 2019. A phylogenomic framework, evolutionary timeline and genomic resources for comparative studies of decapod crustaceans. *Proceedings of the Royal Society B*: *Biological Sciences* **286**:20190079. DOI: https://doi.org/10.1098/rspb.2019.0079

Wolff G, Harzsch S, Hansson BS, Brown S, Strausfeld N. 2012. Neuronal organization of the hemiellipsoid body of the land hermit crab, *Coenobita clypeatus*: correspondence with the mushroom body ground pattern. *Journal of Comparative Neurology* **520**:2824–2846. DOI: https://doi.org/10.1002/cne.23059, PMID: 22547177

Wolff GH, Thoen HH, Marshall J, Sayre ME, Strausfeld NJ. 2017. An insect-like mushroom body in a crustacean brain. *eLife* **6**:e29889. DOI: https://doi.org/10.7554/eLife.29889, PMID: 28949916

Wolff GH, Strausfeld NJ. 2015. Genealogical correspondence of mushroom bodies across invertebrate phyla. *Current Biology* **25**:38–44. DOI: https://doi.org/10.1016/j.cub.2014.10.049, PMID: 25532890

Wolff GH, Strausfeld NJ. 2016. Genealogical correspondence of a forebrain centre implies an executive brain in the protostome–deuterostome bilaterian ancestor. *Philosophical Transactions of the Royal Society B: Biological Sciences* **371**:20150055. DOI: https://doi.org/10.1098/rstb.2015.0055

Yagi R, Mabuchi Y, Mizunami M, Tanaka NK. 2016. Convergence of multimodal sensory pathways to the mushroom body calyx in *Drosophila melanogaster. Scientific Reports* **6**:29481. DOI: 10.1038/srep29481

Yasuyama K, Meinertzhagen IA, Schürmann F-W. 2002. Synaptic organization of the mushroom body calyx in *Drosophila melanogaster*. *Journal of Comparative Neurology* **445**:211–226. doi:10.1002/cne.10155

Terminology

Terms and abbreviations follow recommendations by the insect brain consortium regarding those jointly applicable to insect and crustacean (Pancrustacea) central nervous systems. See Ito et al. (2014). Other terms used for crustacean brain centers follow those of Bellonci (1882) and Sandeman et al. (1993). Other terms are defined in the body of this paper.

Acknowledgements

The research described here is supported by the National Science Foundation under Grants No. 1754798 awarded to NJS. Our gratitude is once again directed to Daniel Kalderon, Columbia University, New York, for supplying the DC0 antibodies, as he has during the last decade and longer. We thank the staff of the University of Washington's Friday Harbor Marine Laboratories, San Juan, for their unfailing help in obtaining living specimens. Briana Olea-Rowe and Hannah Joy Miller provided expert technical assistance. We have profited from discussions and advice from Wulfila Gronenberg (University of Arizona) and Frank Hirth (Kings College, University of London) and are indebted to Camilla Strausfeld for her advice, critically discussing versions of the manuscript, suggesting many improvements and meticulously editing the text.

FIGURE SUPPLEMENTS

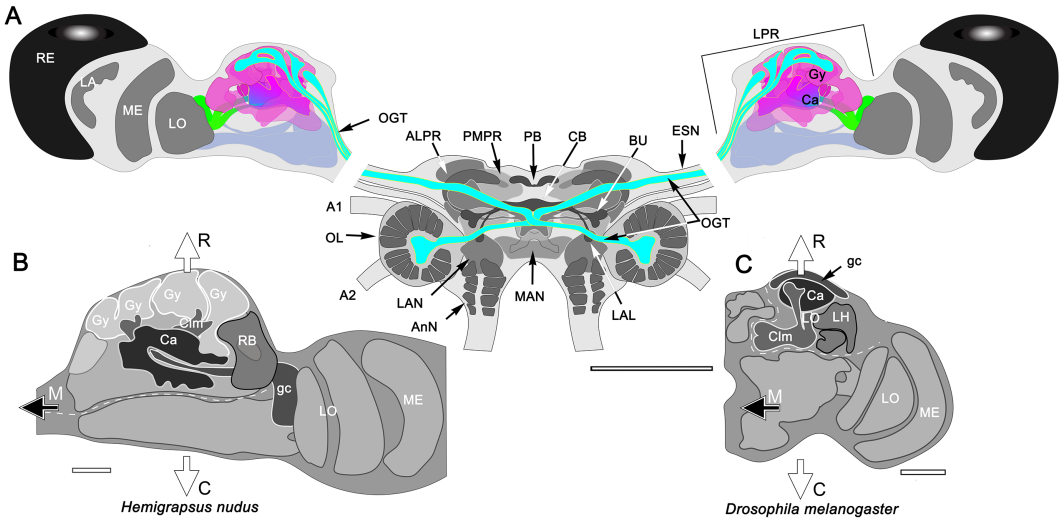

Figure 1 —— figure supplement 1 (a) Schematic of the *Hemigrapsus* brain (frontal view) and major neuropils. Abbreviations: ALPR, anterior lateral protocerebrum; A1, antennule nerve; A2, antennal nerve; AnN, antenna 2 neuropil; BU, lateral bulb of the central complex; CB, central body; ESN, eyestalk nerve; LAL, lateral accessory lobe; LAN, lateral antennular lobe neuropil; LA, lamina; LO, lobula; LPR, lateral protocerebrum; MAN, medial antenna 1 neuropil; MB, mushroom body; ME, medulla; OL, olfactory lobe; OGT, olfactory globular tract; PMPR, posterior medial protocerebral neuropils; PB, protocerebral bridge; RE, compound retina. The eyestalk nerve ESN) carries *all* axons connecting the brain with the lateral protocerebrum. (**b, c**) Orientations of the varunid lateral protocerebrum aligned with that of *Drosophila*. The white dashed lines in *H. nudu*s divides its rostral lateral protocerebral volume from its caudal volume; in *Drosophila* the dashed line divides the rostral volume of the protocerebrum from the rest of the hemi-brain. In both taxa, the filled arrow M indicates medial, and the open arrows R, C indicate, respectively, the rostral and caudal axes. Both schematics depict a view from the ventral side of the lateral protocerebrum/ hemibrain. Abbreviations: Ca, calyces; Clm, column; gc, globuli cells; Gy, gyri; LH, lateral horn; LO, lobula complex; ME, medulla; RB, reniform body; Scale bars: a, 500μm; b–d 100μm

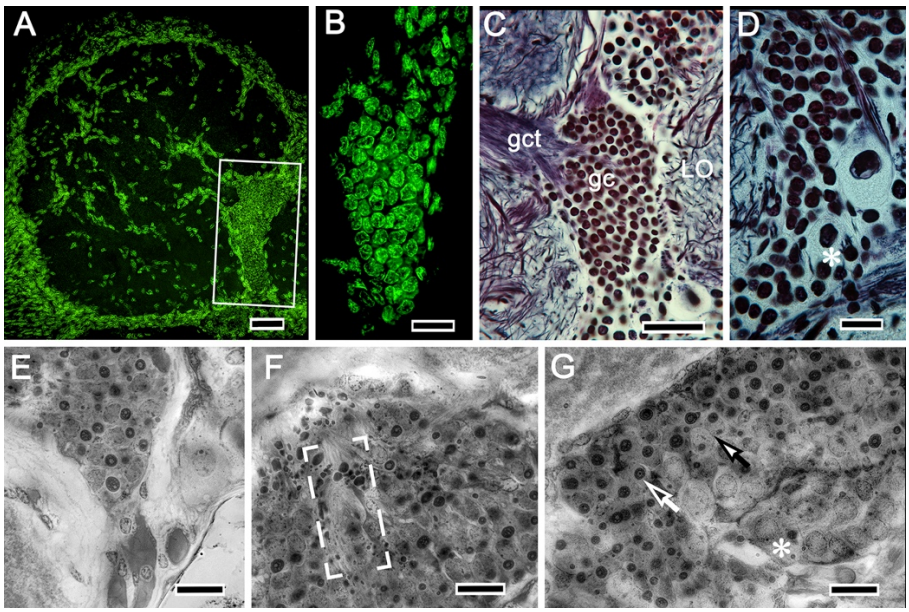

Figure 2 —— figure supplement 1. Globuli cells supplying intrinsic neurons to the mushroom bodies. In the varunid crab, globuli cells occupy a unique location between the distal margin of the lateral protocerebrum and proximal margin of the optic lobe as shown in **A**. (**B**) As is typical of globuli cells in other taxa (insects, shrimps) they are minute, here measuring less than 6 μm diameter, the next largest being reniform perikarya as in panel C, upper right. (**D-G**) Like other decapods, crabs molt and grow throughout life, their brains also increasing in size. The globuli cell cluster evidences neuroblasts (asterisk in panel D), and grouped globuli cells suggesting clonal siblings (**E**). Ganglion mother cells are also arranged as aligned groups (**F**) or, as in panel **G**, dividing (closed arrow) between neuroblasts (asterisk) and fully differentiated perikarya (open arrow). Scale bars, A, 50mm; B, 20μm; C, 50μm; D-G, 20μm.

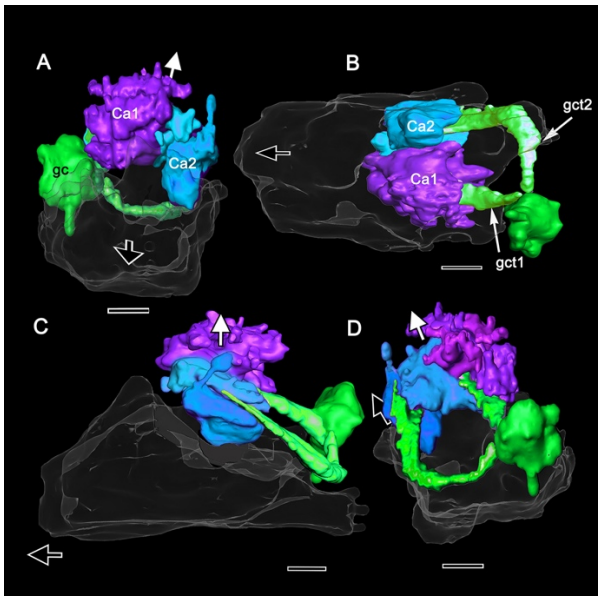

Figure 2 —— figure supplement 2. Globuli cells provide two tracts, one to each calyx as shown in this Amira reconstruction of a serially sectioned osmium-ethyl gallate-treated brain. Two tracts composed of neurites from 2,000-3,000 globuli cells from a unified cluster (gc) extend to two calyces (Ca1, Ca2), Ca1 is dorsal to and larger than Ca2. (**A**) Viewed from above, with the medial margin of the lateral protocerebrum

closest to the observer, the rostral surfaces of each calyx are highly indented with some finger-like extensions reaching upwards. (**B**) viewed from beneath, with the dorsal calyx 1 closest to the observer, the more caudal levels of the calyces are seen to be layered, this distinction between caudal and rostral volumes also shown viewing into the lateral protocerebrum from its ventral surface (C). (**D**) 180º rotation from panel A suggests greater surface elaboration of Ca1 than Ca2.

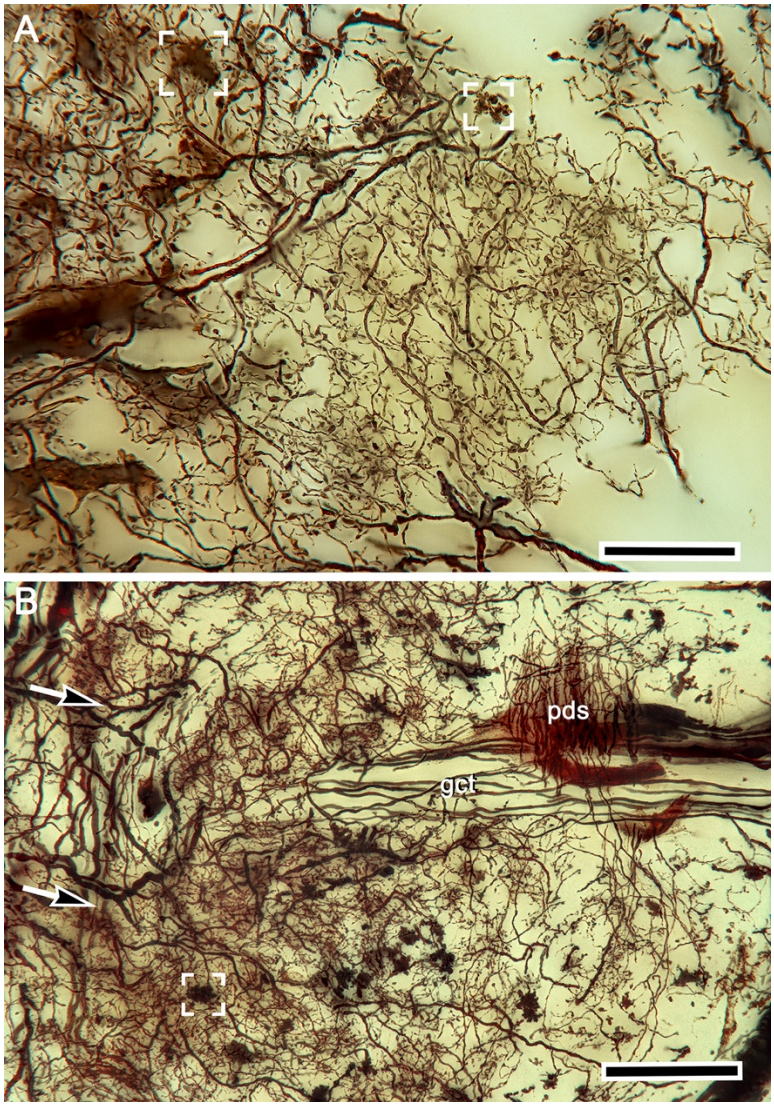

Figure 3 —— figure supplement 1. Rectilinear network organization of the calyx and afferent supply. (**A**) Golgi impregnation showing regular network arrangements of intrinsic cell dendrites. Robust afferent terminals are defined by varicose specializations. A single terminal is shown in the box upper right; several convergent terminals in the box upper left. (**B**) The globuli cell tract (gct) extends medially beneath processes belonging to the reniform body's pedestal (pds). Afferent terminals fibers enter from the left (arrowed) to distribute terminals (one boxed, lower left) amongst densely arranged intrinsic neuron dendrites extending from globuli cell neurites comprising the gct. Scale bars, A, B, 50μm.

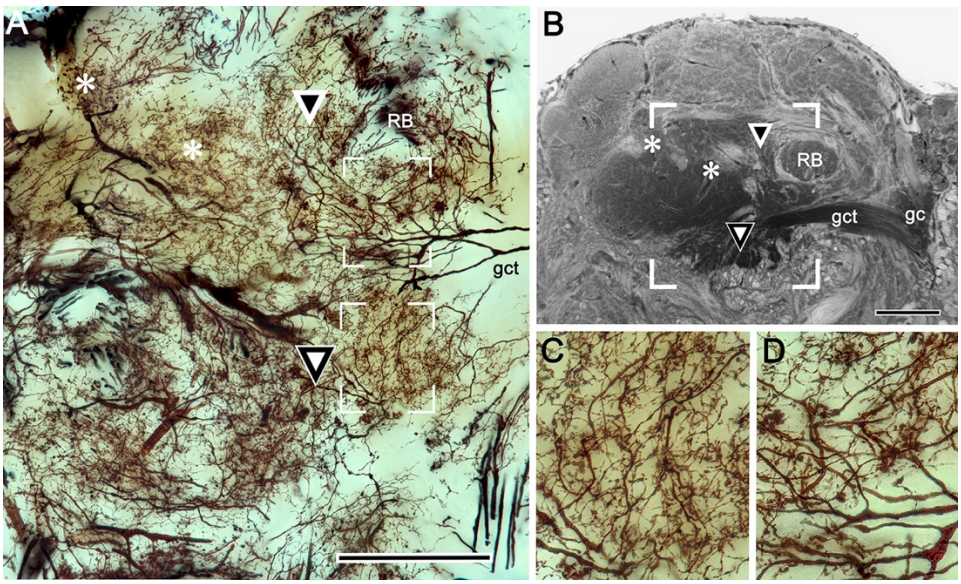

Figure 4 —— figure supplement 1. Fidelity of intrinsic neurons fields (**A**) and calycal domains revealed by osmium-ethyl gallate (**B**). The equivalent of the area in panel **A** is indicated by the open box in panel **B**. Corresponding loci in B and A are indicated by symbols. Boxed areas in **A** are enlarged in panels **C**, **D** showing rectilinear organization of intrinsic processes and their convergence at nodes corresponding to microglomeruli. Abbreviations: RB, reniform pedestal; gc, globuli cells; gct, globuli cell tract. Scale bars, A, B, 100μm

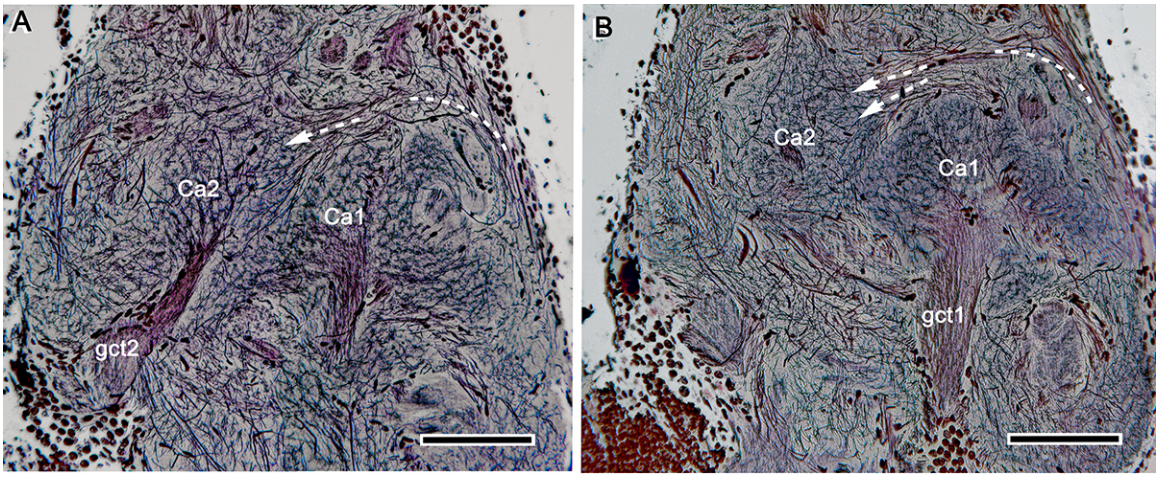

Figure 4 —— figure supplement 2. Calyx distinctions. (**A, B**) Two serial silver-stained sections showing the side-by-side disposition of calyces 1, 2 (Ca1, Ca2) each supplied by its own globuli cell tract (gct1, 2). Arrowed paths indicate passage of axons extending to Ca2 from pathways from the optic lobe medulla and reniform body (far right in both panels). Scale bars, 100μm.

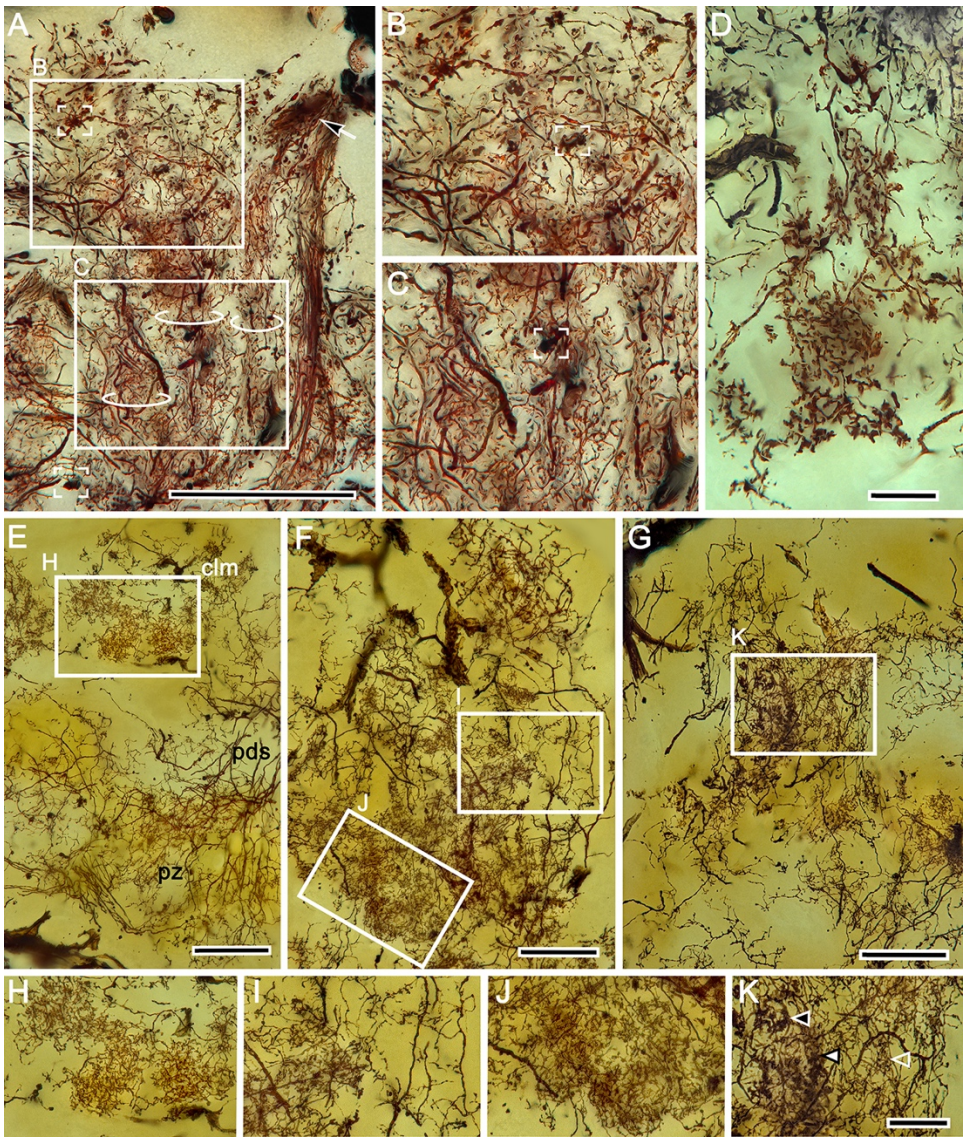

Figure 7 —— figure supplement 1. Intrinsic neuron organization in columns. (**A**) Golgi impregnation of a column originating from calyx 2. Three parallel but distinct ensembles of intrinsic neuron processes (circled) all splay outwards immediately beneath the overlying gyriform neuropil, which is here unstained. Details of these ensembles shown in **B**, **C** demonstrate internal complexity. Of note is the presence of bouton-like terminals (two indicated by box brackets) suggesting either afferent supply from the eyestalk nerve or reciprocal inputs from rostral gyri. A cascade arrangement of processes extending parallel to the column from a more rostral level (arrow) may indicate recurrent afferent supply from the gyri. (**D–G**) Columns also contain what appear to be intrinsic elements (**D**) that do not originate from the calyces, as occurs in the mushroom bodies of certain insects (see Discussion). (**E**) There is a clear distinction between the arrangement of processes (enlarged in **H**) in the columns (clm) and the more distributed arrangements in the proximal zone (pz) of the reniform body indicated by its pedestal (pds). (**F**) Further complexity is demonstrated by parallel arrangements of intrinsic neuron and their collaterals suggestive of local circuits (examples indicated in boxed areas in panel F, enlarged in **I**, **J**). (**G**) Dense arrangements near the column's terminal expansion reveal claw-like specializations each with its particular morphology, within parallel subdivisions of the column (indicated by arrowheads in K). Scale bars, A,100μm; E–G, 25μm; D, H-K, 20μm.

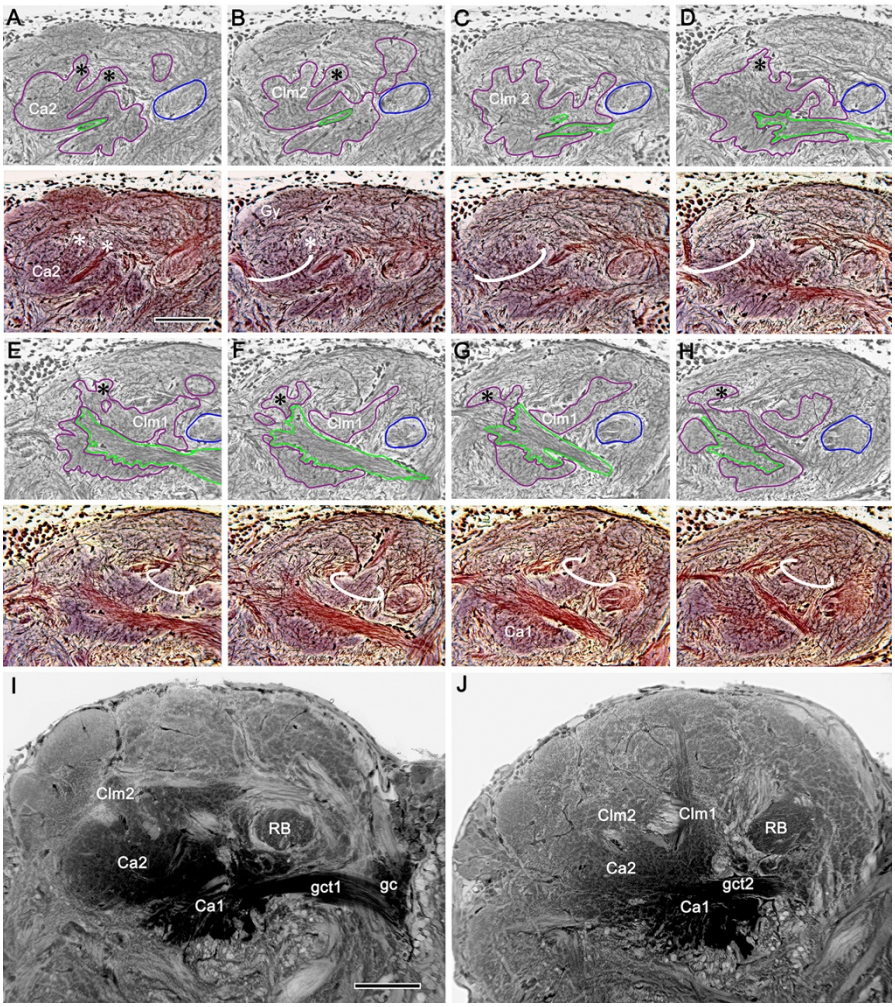

Figure 7 —— figure supplement 2. The interface between columns and gyri. (**A-H**) Paired half-tone/color micrographs of selected levels of a silver-stained, serially sectioned RLPR (medial to the left, rostral upwards). Green outlines in panels A-D indicate parts of the globuli cell tract (gct2) to calyx 2 (Ca2); in E-H, parts of the gct1 to calyx 1 (Ca1). Blue outlines indicate cross–sections of the reniform body pedestal (RB); magenta outlines indicate mushroom bodies (calyces and their columns). Identification of the calyces is enabled by their color and microglomeruli as in Ca2, (lower panel A). As in osmium-ethyl gallate sections, the two calyces are too close to identify separately unless viewed downwards from the rostral surface of the LPR (as in Figure 4 - figure supplement 2). Columns (ringed) and smaller finger-like extensions (asterisks) extend outwards to the gyri. Column 2 (Clm2) from calyx 2 (Ca2) is shown in panels A-D. Panels E-H illustrate the origin and width of Clm1 from Ca1. Panels I and J show corresponding arrangements revealed by osmium-ethyl gallate. Scale bars, 100μm.

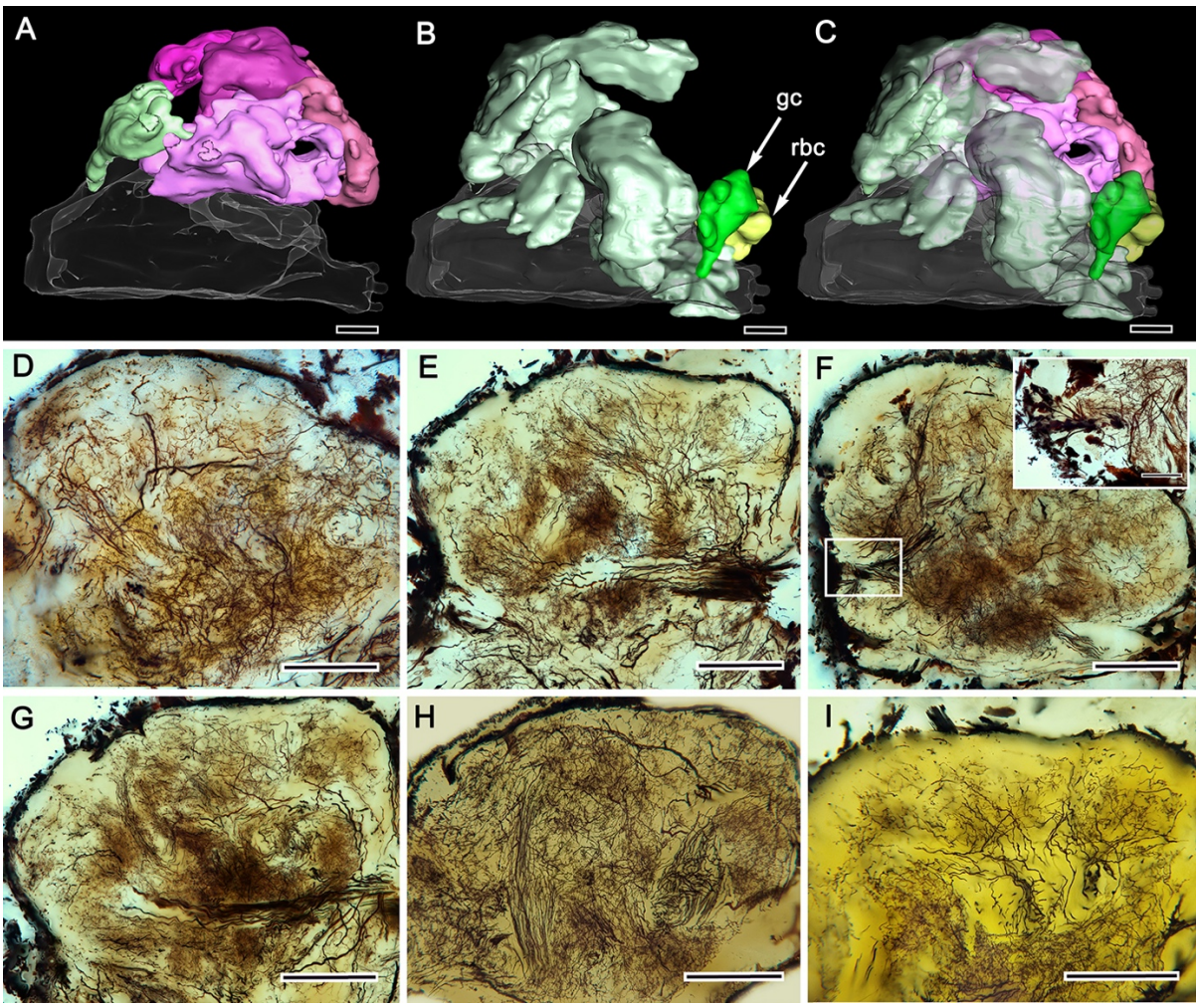

Figure 9 —— figure supplement 1. Perikaryal distributions and gyri neurons. (**A–C**). Amira-generated 3-D reconstruction of the gyri in panel A with the proximal gyrus (light green) above the medial root of the eyestalk nerve. Panel B shows extensive patches of neuronal perikarya, with the globuli cell cluster (gc, dark green) and reniform body cluster (rbc, yellow) situated at the distal margin of the RLPR. Merged images in panel C show the relative dispositions of cell body clusters and gyri. (**D-I**) Stitched reconstructions of Golgi mass impregnations resolve top (rostral)-down (F, H), lateral (E, G, I) and sub-gyrus (D) views of neuropils. The boxed area in F includes cell bodies of a lateral patch, enlarged in the upper right inset. Scale bars, A-I, 100μm, inset to panel F, 25μm.

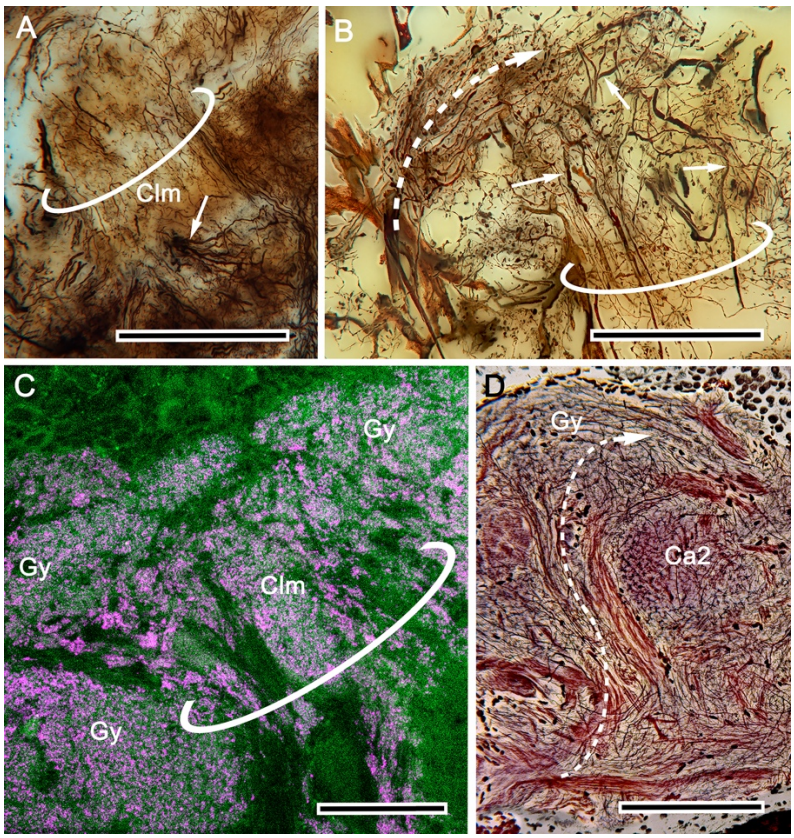

Figure 10 —— figure supplement 1. Column-gyrus interface organization**.** (**A**) Terminus of column 2 from calyx 2 (Clm, circled). The column is notable for its many extremely slender intrinsic processes. Also, visible in this preparation are branches of extrinsic (efferent) neurons extending across the column (arrow). (**B**) Terminus of column 2 (circled) with bundled intrinsic processes and the stouter profiles of efferent neurons (arrowed) ascending from the column into overlying gyral neuropil. This superficial level also receives terminals decorated with small bead-like specializations provided by bundled small-diameter axons from the eyestalk nerve (curved arrow). (**C**) Synapsin (magenta)-actin (green) labelling showing at the terminus of a column (circled) its longitudinal divisions denoted by various sizes and densities of synaptic sites across its width. Similar variation is resolved in flanking neuropil of the gyrus (Gy). (**D**) Reduced silver demonstrates bundles (dashed arrow) from the CLPR ascending outside a column into gyri, demonstrating that multimodal convergence occurs at many levels in the lateral protocerebrum. Part of Ca2 is also visible at this level. Scale bars**,** A, D, 100μm; B, 50μm; C, 25μm.

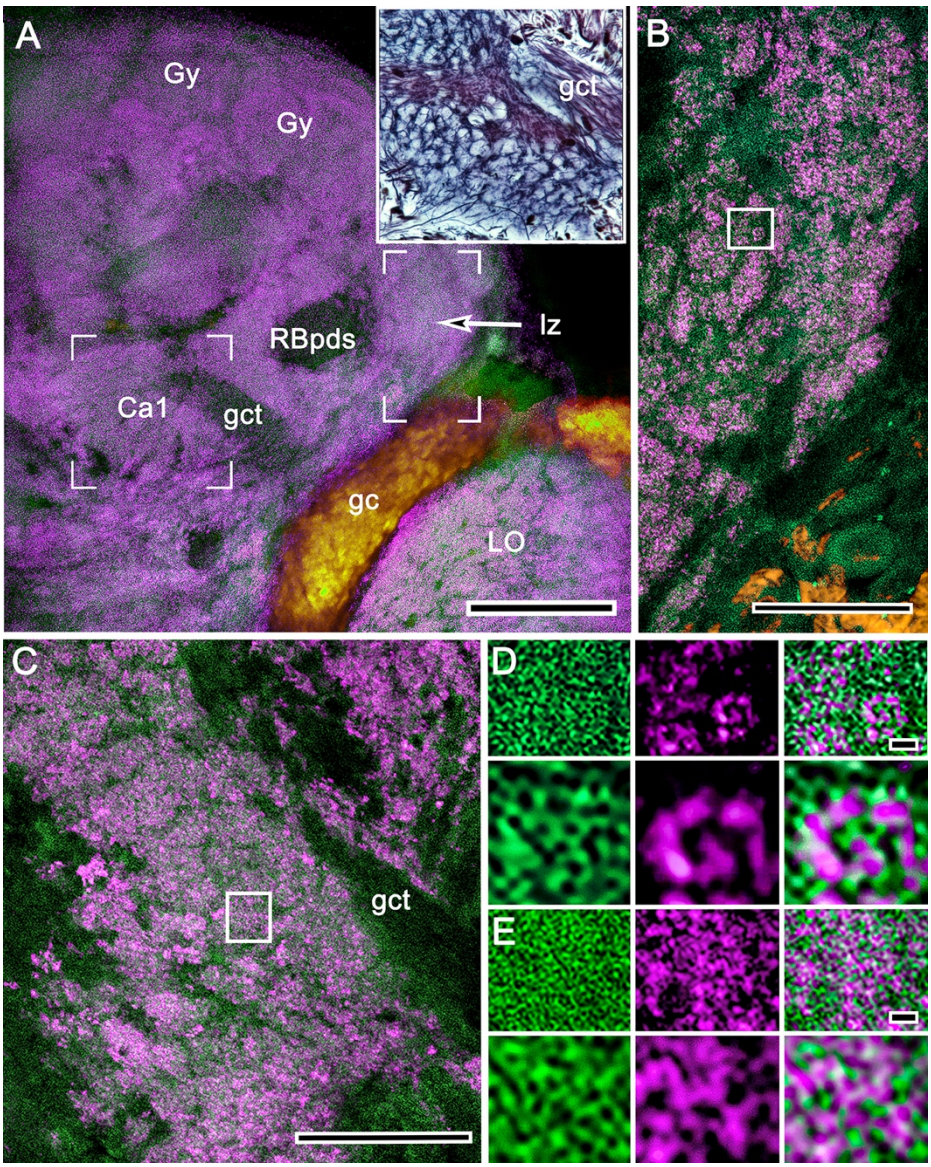

Figure 11 —— figure supplement 1. Comparison of synaptic densities associated with the calyces and reniform body. (**A**) Calyx 1 (Ca1), its associated gyri (Gy), the reniform body pedestal (RBpds) and, at this level, its lateral zone (lz) are shown labelled with actin (green)/anti-synapsin (magenta). In A, the open square corresponds to a similar area of silver-stained microglomeruli (upper right inset). The same area is shown enlarged in panel C. The open rectangle in A is enlarged in B to the same scale as panel C. (**B**) Reniform body neuropils comprise synaptic configurations that contribute to large glomerulus-like islets. (**C**) Microglomeruli of the calyces are smaller and more densely packed than those of the reniform body. (**D, E**) Comparison of synapsin/actin contributions to glomerulus-like units of the reniform body (D) and to microglomeruli of the mushroom body calyx (E) further demonstrates major differences regarding the density of their converging presynaptic elements. Other abbreviations: LO, lobula; gc, globuli cells; gct, globuli cell tract. Scale bars**,** A, 100μm; B,C, 25μm; D, E, 1μm.